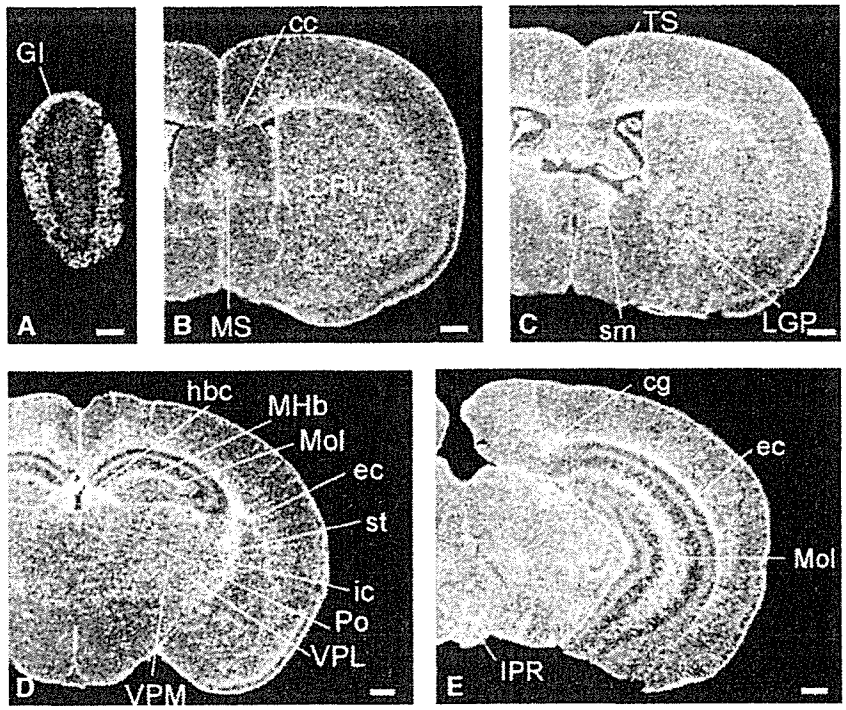

Fig. 4 – Id3 mRNA expression in the brain. Dark field photomicrographs showing Id3 mRNA expression in coronal sections. Strong expression was observed in the medial septal nucleus (B), stria medullaris of the thalamus (C), molecular layer of the dentate gyrus, external capsule, internal capsule (D), and cingulum (E). Scale bar, 500 μm. Abbreviations are listed in Table 1.

was observed in the lateral amygdaloid nucleus dorsolateral part (LaDL), ventromedial part (LaVM), and medial amygdaloid nucleus posterodorsal part (MePD) (Fig. 5C). In the brainstem, Id4 mRNA was expressed in the interpeduncular nucleus, lateral and rostral subnuclei (IPL, IPR), and dorsal raphe nucleus, dorsal and ventral parts (DRD, DRV) (Fig. 5E). These

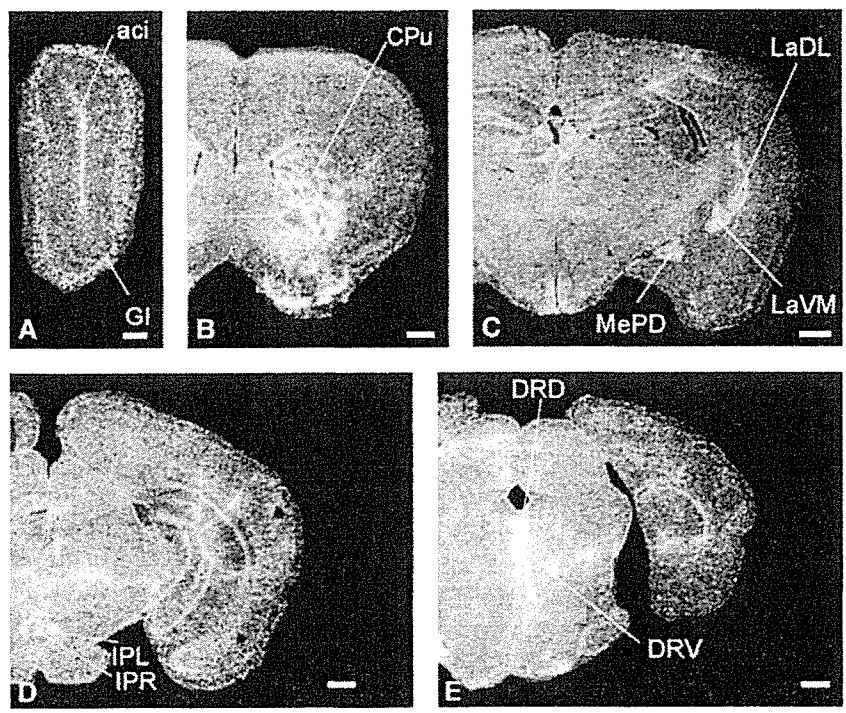

Fig. 5 – Expression of Id4 mRNA in the brain. Dark field photomicrographs showing Id4 mRNA expression in coronal sections. Expression was observed in the caudate putamen (B), lateral amygdaloid nucleus, dorsolateral and ventromedial part, medial amygdaloid nucleus, posterodorsal part (C), interpeduncular nucleus, lateral and rostral subnucleus (D), and dorsal raphe nucleus, dorsal and ventral parts (E). Scale bar, 500 μm. Abbreviations are listed in Table 1.

Table 2 – Summary of Id2 and Id3 expression in the adult mouse brain

	Id2	Id3
Forebrain		
Main olfactory bulb		
Mitral cell layer	++	+
Glomerular layer	++	++
Granule cell layer	+	+
Anterior olfactory nucleus	+	+
Septum		
Lateral septal nucleus	+	+
Medial septal nucleus	–	++
Triangular septal nucleus	–	++
Corpus callosum	+[a]	++
Stria terminalis	–	++
External capsule	–	++
Internal capsule	–	++
Habenular commissure	–	++
Medial habenular nucleus	–	++
Cingulum	–	++
Cerebral cortex		
Neo cortex		
Layer 1	+[a]	+
Layer 2	++	+
Layer 3	++	+
Layer 4	–	+
Layer 5	+++	++
Layer 6	++	++
Amygdaloid complex		
Basolateral, anterior part	+++	+
Lateral		
Dorsolateral part	+++	+
Ventromedial part	+++	+
Ventrolateral part	+++	+
Medial		
Posterodorsal part	+++	+
Posteroventral part	+++	+
Anterior cortical	+++	+
Posteromedial cortical	+++	+
Intercalated nuclei	+++	+
Other subnuclei	++	+
Anterior amygdaloid area	++	+
Hippocampus		
Subgranular zone	++[a]	+
Subiculum	+++	+
Molecular layer	+[a]	+++
Nucleus of the lateral olfactory tract	++	+
Dorsal endopiriform nucleus	+++	+
Bed nucleus of stria terminalis	++	+
Intraamygdaloid division of the bed nucleus of the stria terminalis	++	+
Globus pallidus	++	++
Caudate putamen	+[a]	++[a]
Subventricular zone–ependymal region	++	++
Anterior part of the subventricular zone	+++	+
Ventral pallidum	++	+
Thalamus		
Ventral anterior nucleus	++	+
Ventral posteromedial nucleus	++	++[a]
Ventral posterolateral nucleus	–	++[a]
Posterior thalamic nuclear group	–	++[a]
Geniculate nucleus	++	+
Other subnuclei	+	+
Subthalamic nucleus	++	+
Hypothalamus		
Paraventricular hypothalamic nucleus anterior parvicellular part	++	+
Dorsomedial hypothalamic nucleus	++	+
Other nuclei	+	+
Suprachiasmatic nuclei	++	+
Midbrain		
Substantia nigra		
Pars compacta	–	+
Pars reticulata	++	+
Pars lateralis	–	+
Ventral tegmental area	–	+
Interpeduncular nucleus	++	++
Medial terminal nucleus of the accessory optic tract	+++	+
Red nucleus	++	+
Superior colliculus	++	+
Oculomotor nucleus	+	+
Trochlear nucleus	+	+
Pons		
Pontine nucleus	+++	+
Median raphe nucleus	+	+
Dorsal raphe nucleus	+	+
Periaqueductal gray	+	+
Pontine reticular nucleus, oral part	+	+
Lateral lemniscus	+++	+
Rostral periolivary region	+++	+
Nucleus of the trapezoid body	+++	+
Lateral superior olive	++	+
Periolivary region	++	+
Motor trigeminal nucleus	+	+
Principal sensory trigeminal nucleus	+	+
Lateral vestibular nucleus	++	+
Cochlear nuclei	+++	+
Medulla		
Lateral paragigantocellular nucleus	+	+
Rostroventrolateral reticular nucleus	+	+
Spinal trigeminal nucleus	+	+
Dorsal motor nucleus of the vagus	++	+
Hypoglossal nucleus	+	+
Cerebellum		
Purkinje cells	+++	+
Granule cell layer	–	+
Molecular layer	–	+
Cerebellar nuclei	++	+

Level of expression: +++ high; ++ moderate; + low; – not detected.
[a] Positive cells were scattered.

results revealed that the members of the Id gene family exhibit distinct expression patterns in the adult mouse brain.

The results of the present study are tabulated (Table 2). Since the expression levels of Id1 and Id4 were low, we excluded their results from the table. The present work thus confirmed the previous observations regarding the Id2 gene expression and further demonstrated that Id2 mRNA is distributed more widely throughout the brain. Our study provides evidence that supports the involvement of Id2 in neural functions of the adult brain. In addition, the results for expression of other Id genes imply that the Id gene products play distinct but overlapping roles in the adult mouse brain. Regarding the cell types that express Id2, morphological examination of the specimens counterstained by Nissl staining suggests that most of them are neurons. However, we cannot exclude the possibility that non-neuronal cells also express Id2, depending on the brain regions, because the

present study does not include double labeling with markers for neurons.

In the limbic system, Id2 mRNA was observed in various regions including the piriform, cingulate and retrosplenial cortices, septal nucleus, hippocampus, the bed nucleus of the stria terminalis, and many amygdaloid subnuclei. In the amygdala, Id2 mRNA is expressed moderately in LaDL and LaVM and highly in intercalated cells of the amygdala. The lateral nucleus is the main input station of the amygdala for visual and auditory sensory input (Collins and Pare, 1999; McDonald, 1998), and intercalated cell masses receive inputs from the basolateral complex and project to the central nucleus (Collins and Pare, 1999). Since the amygdala is associated with emotion and behavioral responses, Id2 may play a role in regulating these neural functions.

In the developing mouse brain, Id2 mRNA expression has a boundary in the neocortical layer 5, and the boundary demarcates the transition from the sensory to motor region, suggesting that Id2 is associated with cortical regionalization (Rubenstein et al., 1999). However, in the adult brain, the boundary is not clear in our analysis (data not shown). Id2 may have some function in addition to cortical regionalization. Id2 mRNA was expressed in the cranial nerve nuclei, not only in the motor nuclei, but also the sensory nuclei. As reported previously (Andres-Barquin et al., 2000; Jen et al., 1997; Neuman et al., 1991; Rubenstein et al., 1999; Tzeng and de Vellis, 1998), Id2 mRNA was observed in neurons in the cerebral cortex and caudate putamen. In addition, most cells in the globus pallidus and pars reticulata of the substantia nigra were labeled for Id2 mRNA. These observations suggest the involvement of Id2 in motor functions.

The circadian rhythm in mammals has been thought to be under the control of the pacemaker located in the SCN of the hypothalamus (Inouye and Shibata, 1994). As reported previously (Ueda et al., 2002), Id2 mRNA was detected in SCN in our study. In addition, we found that it was also expressed in the regions of the paraventricular nucleus (PVN) and stria terminalis (BNST). Vasopressin containing pathways from the SCN serve to affect neuroendocrine and autonomic neurons in the PVN (Buijs et al., 1998). GABA and glutamate are important mediators of fast monosynaptic transmission from the SCN to defined neurons in the PVN and are candidates for conveying circadian rhythmicity to PVN regulation of neuroendocrine and autonomic processes (Hermes et al., 1996). The circadian rhythm of electrical activity in the bed nucleus of the BNST is in phase with the SCN electrical activity rhythm (Yamazaki et al., 1998). Thus, Id2 may be involved in the regulation of circadian rhythm. In accordance with this notion, Id2 expression in the SCN is high during circadian night (Ueda et al., 2002).

It is known that two regions contain neural stem cells in the adult rodent brain: the subgranular zone (SGZ) of the hippocampal dentate gyrus and the subventricular zone (SVZ) (Altman and Bayer, 1990; Doetsch et al., 1999; Eriksson et al., 1998; Goldman, 1998; Johansson et al., 1999). The SGZ is the source of granule cells in the hippocampus produced during the juvenile and adult periods (Altman and Bayer, 1990), and the anterior part of the subventricular zone (SVZa) is a source of neuronal progenitor cells for the olfactory bulb (Luskin, 1993). In this study, we found that Id2 mRNA was expressed in the SVZa. Id2 may be related to the production of neurons in the olfactory bulb. This notion is consistent with the physiological activity of Id proteins because Id proteins are thought to function to expand and maintain the immature cells.

Acknowledgments

We are grateful to M. Sato for sharing equipment and D. Nathans and F. Sablitzky for materials. This work was supported by Grants-in-Aid and by the 21st Century COE program "Biomedical Imaging Technology Integration Program" from the Japan Society for the Promotion of Science.

REFERENCES

Altman, J., Bayer, S.A., 1990. Migration and distribution of two populations of hippocampal granule cell precursors during the perinatal and postnatal periods. J. Comp. Neurol. 301, 365–381.

Andres-Barquin, P.J., Hernandez, M.C., Israel, M.A., 2000. Id genes in nervous system development. Histol. Histopathol. 15, 603–618.

Benezra, R., Davis, R.L., Lockshon, D., Turner, D.J., Weintraub, H., 1990. The protein Id: a negative regulator of helix–loop–helix DNA binding proteins. Cell 61, 49–59.

Buijs, R.M., Hermes, M.H., Kalsbeek, A., 1998. The suprachiasmatic nucleus–paraventricular nucleus interactions: a bridge to the neuroendocrine and autonomic nervous system. Prog. Brain Res. 119, 365–382.

Christy, B.A., Sanders, L.K., Lau, L.F., Copeland, N.G., Jenkins, N.A., Nathans, D., 1991. An Id-related helix–loop–helix protein encoded by a growth factor-inducible gene. Proc. Natl. Acad. Sci. U. S. A. 88, 1815–1819.

Collins, D.R., Pare, D., 1999. Reciprocal changes in the firing probability of lateral and central medial amygdala neurons. J. Neurosci. 19, 836–844.

Doetsch, F., Caille, I., Lim, D.A., Garcia-Verdugo, J.M., Alvarez-Buylla, A., 1999. Subventricular zone astrocytes are neural stem cells in the adult mammalian brain. Cell 97, 703–716.

Elliott, R.C., Khademi, S., Pleasure, S.J., Parent, J.M., Lowenstein, D. H., 2001. Differential regulation of basic helix–loop–helix mRNAs in the dentate gyrus following status epilepticus. Neuroscience 106, 79–88.

Eriksson, P.S., Perfilieva, E., Bjork-Eriksson, T., Alborn, A.M., Nordborg, C., Peterson, D.A., Gage, F.H., 1998. Neurogenesis in the adult human hippocampus. Nat. Med. 4, 1313–1317.

Goldman, S.A., 1998. Adult neurogenesis: from canaries to the clinic. J. Neurobiol. 36, 267–286.

Hermes, M.L., Coderre, E.M., Buijs, R.M., Renaud, L.P., 1996. GABA and glutamate mediate rapid neurotransmission from suprachiasmatic nucleus to hypothalamic paraventricular nucleus in rat. J. Physiol. 496, 749–757.

Inouye, S.T., Shibata, S., 1994. Neurochemical organization of circadian rhythm in the suprachiasmatic nucleus. Neurosci. Res. 20, 109–130.

Ishii, K., Oda, Y., Ichikawa, T., Deguchi, T., 1990. Complementary DNAs for choline acetyltransferase from spinal cords of rat and mouse: nucleotide sequences, expression in mammalian cells, and in situ hybridization. Brain Res. Mol. Brain Res. 7, 151–159.

Jen, Y., Manova, K., Benezra, R., 1996. Expression patterns of Id1, Id2, and Id3 are highly related but distinct from that of Id4 during mouse embryogenesis. Dev. Dyn. 207, 235–252.

Jen, Y., Manova, K., Benezra, R., 1997. Each member of the Id Gene family exhibits a unique expression pattern in mouse gastrulation and neurogenesis. Dev. Dyn. 208, 92–106.

Johansson, C.B., Momma, S., Clarke, D.L., Risling, M., Lendahl, U., Frisen, J., 1999. Identification of a neural stem cell in the adult mammalian central nervous system. Cell 96, 25–34.

Kageyama, R., Nakanishi, S., 1997. Helix–loop–helix factors in growth and differentiation of the vertebrate nervous system. Curr. Opin. Genet. Dev. 7, 659–665.

Luskin, M.B., 1993. Restricted proliferation and migration of postnatally generated neurons derived from the forebrain subventricular zone. Neuron 11, 173–189.

Massari, M.E., Murre, C., 2000. Helix–loop–helix proteins: regulators of transcription in eucaryotic organisms. Mol. Cell. Biol. 20, 429–440.

McDonald, A.J., 1998. Cortical pathways to the mammalian amygdala. Prog. Neurobiol. 55, 257–332.

Mori, S., Nishikawa, S.I., Yokota, Y., 2000. Lactation defect in mice lacking the helix–loop–helix inhibitor Id2. EMBO J. 19, 5772–5781.

Neuman, T., Keen, A., Zuber, M.X., Kristjansson, G.I., Gruss, P., Nornes, H.O., 1991. Neuronal expression of regulatory helix–loop–helix factor Id2 gene in mouse. Dev. Biol. 160, 186–195.

Paxinos, G., Franklin, K., 2001. The Mouse Brain in Stereotaxic Coordinates, 2nd ed. Academic Press, San Diego, CA.

Riechmann, V., van Cruchten, I., Sablitzky, F., 1994. The expression pattern of Id4, a novel dominant negative helix–loop–helix protein, is distinct from Id1, Id2 and Id3. Nucleic Acids Res. 22, 749–755.

Rubenstein, J.L.R., Anderson, S., Shi, L., Miyashita-Lin, E., Bulfone, A., Hevner, R., 1999. Genetic control of cortical regionalization and connectivity. Cereb. Cortex 9, 524–532.

Ruzinova, M.B., Benezra, R., 2003. Id proteins in development, cell cycle and cancer. Trends Cell Biol. 12, 410–418.

Tzeng, S.F., de Vellis, J., 1998. Id1, Id2, and Id3 gene expression in neural cells during development. Glia 24, 372–381.

Ueda, H.R., Chen, W., Adachi, A., Wakamatsu, H., Hayashi, S., Takasugi, T., Nagano, M., Nakahama, K., Suzuki, Y., Sugano, S., Iino, M., Shigeyoshi, Y., Hashimoto, S., 2002. A transcription factor response element for gene expression during circadian night. Nature 418, 534–539.

Yamazaki, S., Kerbeshian, M.C., Hocker, C.G., Block, G.D., Menaker, M., 1998. Rhythmic properties of the hamster suprachiasmatic nucleus in vivo. J. Neurosci. 18, 10709–10723.

Yokota, Y., Mori, S., 2002. Role of Id family proteins in growth control. J. Cell. Physiol. 190, 21–28.

ELSEVIER

Neurobiology of Disease

www.elsevier.com/locate/ynbdi
Neurobiology of Disease 23 (2006) 169 – 177

Conditional knockout of Mn superoxide dismutase in postnatal motor neurons reveals resistance to mitochondrial generated superoxide radicals

Hidemi Misawa,[a,b,*] Kazuko Nakata,[a] Junko Matsuura,[a] Yasuhiro Moriwaki,[b] Koichiro Kawashima,[b] Takahiko Shimizu,[c] Takuji Shirasawa,[c] Ryosuke Takahashi[d,e]

[a]*Department of Neurology, Tokyo Metropolitan Institute for Neuroscience, 2-6, Musashidai, Fuchu-shi, Tokyo 183-8526, Japan*
[b]*Department of Pharmacology, Kyoritsu University of Pharmacy, 1-5-30, Shibakoen, Minato-ku, Tokyo 105-8512, Japan*
[c]*Department of Molecular Gerontology, Tokyo Metropolitan Institute of Gerontology, 35-2, Sakae-cho, Itabashi-ku, Tokyo 173-0015, Japan*
[d]*Laboratory for Motor System Neurodegeneration, RIKEN Brain Science Institute, 2-1, Hirosawa, Wako-shi, Saitama 351-0198, Japan*
[e]*Deparment of Neurology, Graduate School of Medicine, Kyoto University, 54, Sho-goin kawaramachi, Sakyo-ku, Kyoto 606-8507, Japan*

Received 22 November 2005; revised 24 January 2006; accepted 27 February 2006
Available online 3 May 2006

Mitochondrial dysfunction and oxidative damage are implicated in the pathogenesis of neurodegenerative disease. Mice deficient in the mitochondrial form of superoxide dismutase (SOD2) die during embryonic or early postnatal development, precluding analysis of a pathological role for superoxide in adult tissue. Here, we generated postnatal motor neuron-specific SOD2 knockouts by crossing mice with floxed SOD2 alleles to VAChT-Cre transgenic mice in which Cre expression is restricted to postnatal somatomotor neurons. SOD2 immunoreactivity was specifically lost in a subset of somatomotor neurons resulting in enhanced superoxide production. Yet extensive histological examination revealed no signs of oxidative damage in animals up to 1 year after birth. However, disorganization of distal nerve axons following injury was accelerated in SOD2-deficient motor neurons. These data demonstrate that postnatal motor neurons are surprisingly resistant to oxidative damage from mitochondrial-derived superoxide radicals, but that such damage may sensitize axons to disorganization following nerve injury.

Keywords: Motor neurons; Oxidative stress; Mitochondria; Nerve injury; Conditional knockout; SOD2; Amyotrophic lateral sclerosis

Introduction

Oxygen radicals, of which superoxide ($O_2^{\bullet -}$) is the most abundant, are a natural byproduct of oxygen consumption by the respiratory chain in aerobic ATP production. The superoxide dismutases (SODs) are enzymes that catalyze the conversion of $O_2^{\bullet -}$ to hydrogen peroxide and thus help prevent the build up of toxic $O_2^{\bullet -}$ levels. Three SOD isoforms are expressed in mammalian cells: copper/zinc SOD (SOD1) located in the cytoplasm (McCord and Fridovich, 1969), manganese SOD (SOD2) located in the mitochondrial matrix (Weisiger and Fridovich, 1973) and extracellular SOD (SOD3) (Marklund, 1982; Hjalmarsson et al., 1987). A small fraction of SOD1 is also reported to reside in the intermembrane space of mitochondria (Okado-Matsumoto and Fridovich, 2001; Mattiazzi et al., 2002; Okado-Matsumoto and Fridovich, 2002).

Oxidative stress has been implicated in various neurodegenerative diseases including Parkinson's disease, Alzheimer's disease and amyotrophic lateral sclerosis (ALS). Though it remains unclear whether oxidative stress is a major cause or merely a consequence of cellular dysfunction associated with neurodegenerative diseases (Andersen, 2004), an accumulating body of evidence implicates impaired mitochondrial energy production and increased mitochondrial oxidative damage in early pathological events leading to neurodegeneration (Beal, 1996). Mitochondria are both a major source of reactive oxygen species (ROS) production as well as a major target of ROS-induced cellular injury. Thus, mitochondrial localized superoxide dismutase (SOD2) is thought to play an important role in cellular defense against oxidative damage by ROS.

Loss of SOD2 results in embryonic or early postnatal lethality that varies with genetic background. SOD2 knockout mice on a CD-1 background die either in utero or within 24 h after birth from severe dilated cardiomyopathy (Li et al., 1995). Similarly, C57BL/6 SOD2 knockout mice die at late embryonic or early neonatal stages from dilated cardiomyopathy (Huang et al., 2001; Ikegami et al., 2002). On a mixed C57BL/6 and 129/Sv background, SOD2 mutant mice survive for up to 18 days, develop a milder form of

* Corresponding author. Department of Pharmacology, Kyoritsu University of Pharmacy, 1-5-30, Shibakoen, Minato-ku, Tokyo 105-8512, Japan. Fax: +81 3 5400 2698.
E-mail address: misawa-hd@kyoritsu-ph.ac.jp (H. Misawa).
Available online on ScienceDirect (www.sciencedirect.com).

0969-9961/$ - see front matter © 2006 Elsevier Inc. All rights reserved.
doi:10.1016/j.nbd.2006.02.014

dilated cardiomyopathy and display a neurological phenotype (Lebovitz et al., 1996). In contrast, DBA/2J (D2) SOD2 mutant mice do not develop cardiomyopathy but instead develop severe metabolic acidosis and survive an average of 8 days (Huang et al., 2001). This phenotypic variation suggests that sensitivities to SOD2 deficiency are highly dependent on genetic modifiers that differ across strain and cell type.

Motor neurons are believed to be particularly susceptible to oxidative damage given the high metabolic requirement to sustain a large cell size and long axonal processes. Although motor neurons in cell culture are vulnerable to cell death mediated via calcium influx after exposure to glutamate, it is unclear how motor neurons respond to the overproduction of mitochondrial-derived ROS in vivo. To circumvent the early lethality of SOD2 knockout mice, we used a conditional gene deletion approach in which mice with floxed SOD2 genes (Ikegami et al., 2002) were mated with VAChT-Cre mice (Misawa et al., 2003) that express Cre recombinase in approximately 50% of postnatal somatic motor neurons. Here, we report that conditional loss of SOD2 in postnatal motor neurons results in elevated mitochondrial oxidative stress that fails to trigger signs of neurodegeneration under nonpathological conditions. In contrast, nerve axotomy revealed accelerated nerve disorganization, suggesting that adult motor neurons have relative resistance to mitochondrial-generated superoxide radicals unless stressed.

Materials and methods

Mice

C57BL/6 mice carrying the VAChT-Cre transgene (VAChT-Cre.Fast and VAChT-Cre.Slow) have been described previously (Misawa et al., 2003). C57BL/6 mice with floxed SOD2 alleles have been described elsewhere (Ikegami et al., 2002). Localization of the VAChT-Cre transgene in the VAChT-Cre.Slow mouse line to chromosome 4 was determined by FISH analysis (data not shown), and VAChT-Cre.Slow mice were used to direct motor neuron-specific Cre expression in this study. Homozygous floxed SOD2 mice (lox/lox) were crossed with VAChT-Cre.Slow heterozygote animals. The resulting double heterozygote animals ($SOD2^{lox/+}$; $Cre^{slow/-}$) were selected and mated with homozygote floxed SOD2 mice. All animals were genotyped for SOD2 allele (Ikegami et al., 2002) and the Cre transgene (Misawa et al., 2003) using tail DNA as described previously. Motor performance was analyzed using a rotarod treadmill (MK-600; Muromachi Kikai, Tokyo, Japan) at 28 rpm. Grip strength was measured using a Grip Strength Meter for Mouse (Model 57106; Stoelting, Wood Dale, IL). All animal protocols were approved by the Tokyo Metropolitan Institute for Neuroscience Institutional Animal Care and Use Committee.

Histological assessment and immunohistochemistry

Mice were anesthetized with sodium pentobarbital and perfused through the aortic cone with phosphate-buffered saline (PBS), followed with 4% paraformaldehyde (PFA) in 0.1 M phosphate buffer (PB) at pH 7.4. Brains and spinal cords were removed and postfixed in the same fixative for 2 h and then immersed in 20% sucrose in PB overnight at 4°C. The tissue was sectioned at 20 μm on a freezing microtome. For paraffin-embedded section, tissues were transferred to 70% ethanol and embedded in paraffin as described (Ichikawa et al., 1997). Serial brain or spinal cord sections were cut at 5 μm. Sections were stained for Nissl substance with cresyl violet or Fluoro-Jade B (Chemicon) according to the manufacturer's protocol. For staining of SOD2, SOD1, ChAT, and CHT, paraffin-embedded sections were immunohistochemically processed as described elsewhere (Ichikawa et al., 1997) with diaminobenzidine (DAB) as a chromogen followed by poststaining with hematoxylin. Antibodies used are rabbit polyclonal anti-SOD2 antibody (1:2000; Stressgen Biotechnologies), rabbit polyclonal anti-SOD1 antibody (1:2000; Stressgen Biotechnologies), rabbit polyclonal anti-ChAT (1:10,000; Ichikawa et al., 1997), and rabbit polyclonal anti-CHT antibody (50 ng/ml; Misawa et al., 2001). To estimate frequencies of Cre-mediated recombination of the floxed SOD2 alleles, serial paraffin sections were stained with SOD2 and ChAT as above, and the number of positive cells was counted. More than 500 cells were analyzed in the spinal cord ventral horn and 200 cells in each of the brainstem motor nucleus (from at least 3 mice at respective age). Double labeling for SOD2 and SMI-32 was performed by immunofluorescence. Sections were incubated simultaneously with rabbit polyclonal anti-SOD2 antibody (1:500; Stressgen Biotechnologies) and mouse SMI-32 monoclonal antibody to neurofilaments (1:1,000; Sternberger Monoclonals). Texas red-conjugated goat anti-mouse IgG was used to detect SMI-32-positive cells, and fluorescein isothiocyanate-conjugated goat anti-rabbit IgG was used to detect SOD2-expressing cells (1:200; Jackson Immunoresearch Labs).

In situ detection of $O_2^{\bullet -}$ production

The spatial production of $O_2^{\bullet -}$ was investigated by in situ detection of oxidized hydroethidine (HEt; Molecular Probes) as previously described (Murakami et al., 1998). HEt is oxidized to a red fluorescent dye (ethidium) in living cells selectively by $O_2^{\bullet -}$, but not by other reactive oxygen species such as hydrogen peroxide, hydroxyl radical, or peroxynitrite (Bindokas et al., 1996). Briefly, HEt solution (0.2 ml; stock solution of HEt, 100 mg/ml in DMSO, diluted to 1 mg/ml in PBS) was intravenously injected 30 min before the animals were sacrificed. The animals were perfused with 4% paraformaldehyde as described above. Brain and spinal cord sections (20 μm) were cut on a cryostat and processed for fluorescent microscopy.

Hypoglossal nerve axotomy

Nine-month-old mice ($SOD2^{lox/lox}$;$Cre^{slow/-}$ or $SOD2^{lox/lox}$;$Cre^{-/-}$) were anesthetized with an intraperitoneal injection of ketamine (80 mg/kg) and xylazine (12 mg/kg). The right hypoglossal nerve was exposed under the digastric muscle and transected with scissors. After 5 weeks, the animals were reanesthetized and perfused with 4% paraformaldehyde. The brainstem was removed, 5-μm serial paraffin-embedded sections were prepared and stained with cresyl violet as described above. Hypoglossal motor neurons with distinct clear nuclei in every eighth section (total 8 sections per animal) were counted.

Analysis of Wallerian degeneration

Two days after unilateral transection of hypoglossal nerves as described above, mice were sacrificed by over-dose of sodium pentobarbital, the swollen first 2 mm of the distal nerve was discarded, the next 2 mm was used for morphological analysis, and a segment 4–7 mm distal to the lesion site was used for Western blotting. For morphological analysis, the nerve segments were fixed

for 1 day in 2% paraformaldehyde, 2% glutaraldehyde in 50 mM phosphate buffer, pH 7.4 (PB). Samples were treated in 1% OsO_4 in PB, washed, dehydrated with ethanol and then propylene oxide, and finally embedded in Quetol 812 epoxy resin (Nisshin EM, Tokyo, Japan). Semithin cross-sections (0.5 μm) for light microscopy were stained with toluidine blue.

Electron microscopy

Animals were perfused with 2% glutaraldehyde, 2% paraformaldehyde, 5% sucrose in 50 mM phosphate buffer (pH 7.4). The brain and spinal cord were removed and postfixed in the same fixative for 1 d at 4°C. The facial nucleus and spinal cord ventral horn were cut into 1- to 2-mm square pieces, fixed in 1% osmium tetroxide for 1 h at 4°C, dehydrated through a graded series of ethanol solutions and into propylene oxide, and embedded in Quetol 812 (Nissin EM). Ultra-thin sections were stained with lead citrate and uranyl acetate and examined with an electron microscope (H7500; Hitachi, Tokyo, Japan) at 10,000× magnification.

Analysis of muscle atrophy and denervation

Fresh skeletal muscle biopsies were obtained and frozen by immersion in isopentane cooled in liquid nitrogen. Sections were

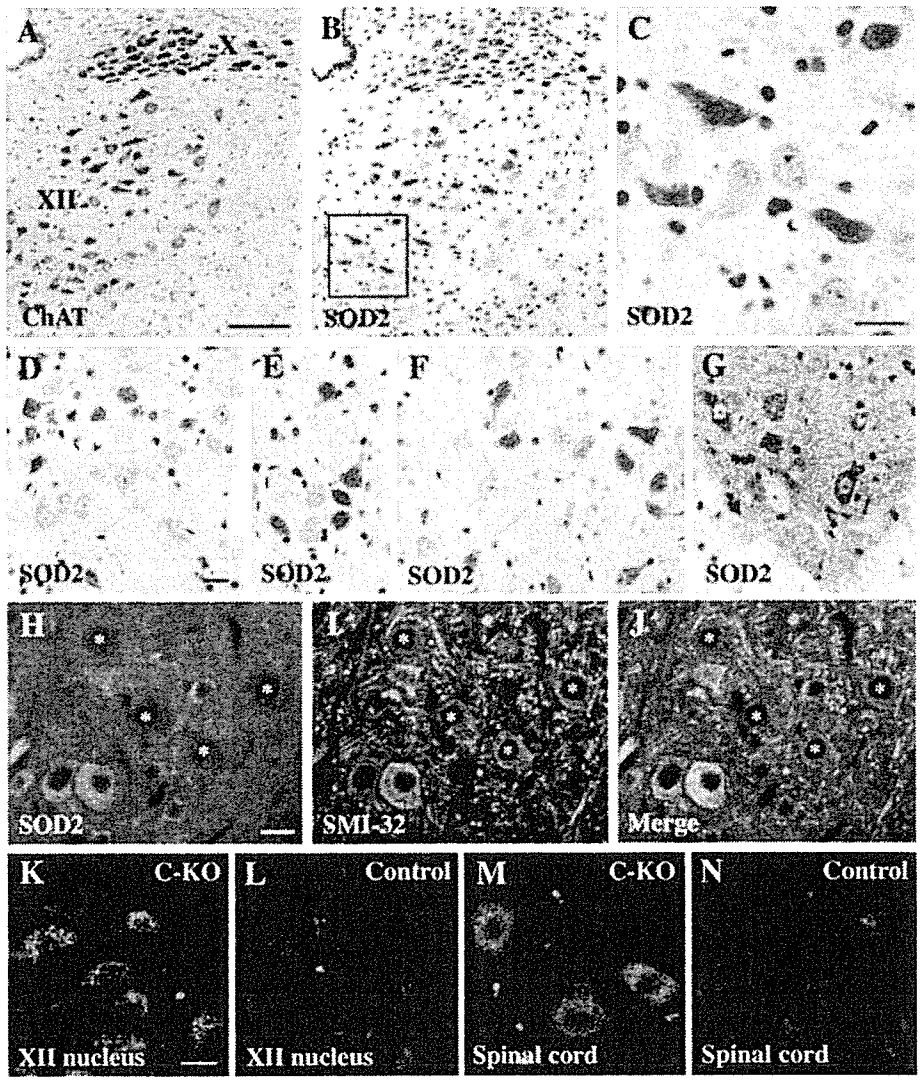

Fig. 1. Loss of SOD2 immunoreactivity in motor neurons from $SOD2^{lox/lox}$;$Cre^{slow/-}$ mice. (A–G) Paraffin-embedded sections of brain and spinal cord from $SOD2^{lox/lox}$;$Cre^{slow/-}$ mice at 5 months old stained with anti-ChAT antibody (A) or anti-SOD2 antibody (B-G). SOD2 immunoreactivity was lost in a subset of ChAT-positive somatomotor neurons as revealed by serial section through the hypoglossal nuclei (A–C) as well as sections through the oculomotor (D), abducens (E), facial (F) nuclei, and the ventral horn of the spinal cord (G). Note that SOD2 immunoreactivity was preserved in visceromotor neurons in the dorsal motor nucleus of the vagus (B). X, dorsal motor nucleus of the vagus; XII, hypoglossal nucleus. The boxed area in B is enlarged in panel C. (H–J) Paraffin-embedded sections from the ventral horn of the spinal cord were double-stained by immunofluorescence with anti-SOD2 (H) and anti-SMI-32 (I) antibodies. The merged image is shown in panel J. SOD2 immunoreactivity was lost in a subset of SMI-32-positive large motor neurons (denoted by asterisks) but not in SMI-32-negative small-diameter interneurons. (K–N) Mitochondrial production of $O_2^{\bullet -}$ was increased in $SOD2^{lox/lox}$;$Cre^{slow/-}$ (C-KO) mice compared with $SOD2^{lox/lox}$;$Cre^{-/-}$ (Control) mice in motor neurons in the hypoglossal nucleus (K and L) and ventral horn of the spinal cord (M and N) as revealed by HEt oxidation. HEt signals were detected in motor neurons as small granular particles in the cytosol, indicating mitochondrial production of $O_2^{\bullet -}$ under normal physiological conditions. Scale bars = 100 μm (A; also applies to B); 20 μm (C); 20 μm (D; also applies to E–G); 20 μm (H; also applies to I, J); 20 μm (K; also applies to L–N).

cut at 10 μm and processed for hematoxylin–eosin (H&E) or Gomori trichrome staining.

Western blotting

Cytoskeletal protein preservation was determined as described by Mack et al. (2001). Briefly, axotomized or control (uncut) hypoglossal nerves (3-mm length) were homogenized in 50 μl 25 mM Tris–HCl (pH 7.5), 2% SDS, 1 mM EDTA, 1× Complete protease inhibitor cocktail (Roche). Proteins (20 μl each) were separated using a 5–20% gradient polyacrylamide-SDS gel and semi-dry transferred onto a nylon membrane (Immobilon-P; Millipore). Loading and transfer were checked by staining with Ponceau S (Sigma). The membranes were incubated with monoclonal N52 antibody (Sigma) against neurofilament heavy chain diluted at 1:3000 in 5% nonfat skim milk/0.1% Tween 20 in PBS, followed by incubation with horseradish peroxidase-conjugated anti-mouse IgG (Bio-Rad), and visualized with ECL Western Blotting Detection Reagent (Amersham Pharmacia Biosciences). The same blots were reprobed with monoclonal antibody β-tub 2.1 (1:10,000; Sigma) against β-tubulin. In order to compare SOD2 expression between $SOD2^{lox/lox}$;$Cre^{slow/-}$ and $SOD2^{lox/lox}$;$Cre^{-/-}$ mice, ventral halves of the cervical spinal cord (5-mm length) were micro-dissected, homogenized, and processed for immunoblot analysis as described above with rabbit polyclonal anti-SOD2 antibody (1:10,000; Stressgen Biotechnologies), rabbit polyclonal anti-SOD1 antibody (1:10,000; Stressgen Biotechnologies), and mouse monoclonal anti-actin antibody (1 μg/ml; Chemicon).

Results

Generation of motor neuron-specific SOD2 knockout mice

To generate postnatal motor neuron-specific SOD2 knockout mice, we crossed mice homozygous for floxed SOD2 alleles (Ikegami et al., 2002) with VAChT-Cre.Slow mice in which Cre expression is restricted in postnatal somatomotor neurons (Misawa et al., 2003). The VAChT-Cre.Fast line was not used in this study because the transgene integrated on the same chromosome as SOD2 (chromosome 17). Double heterozygote animals ($SOD2^{lox/+}$;$Cre^{slow/-}$) were again mated with homozygous floxed SOD2 mice. $SOD2^{lox/lox}$;$Cre^{slow/-}$ mice were born at a Mendelian ratio and survived to adulthood with no gross defects (data not shown). Furthermore, no signs of motor deficits, including tremor and paralysis, or muscle weakness were observed for up to 12 months as revealed by a rotarod test and grip strength measurements, respectively. Motor neurons in $SOD2^{lox/lox}$;$Cre^{slow/-}$ mice showed normal cell morphology, including soma size, and normal immunoreactivity for cholinergic markers such as choline acetyltransferase (ChAT; Figs. 1A and 2A–F), vesicular acetylcholine transporter (VAChT) and high-affinity choline transporter (CHT). In the brain stem and spinal cord, approximately 50% of ChAT-positive motor neurons lost mitochondrial SOD2 immunoreactivity, suggesting successful targeting of the SOD2 gene (Figs. 1A–J). The SOD2-negative motor neurons were observed in various somatomotor nuclei of the brainstem and spinal cord, but not in visceromotor nuclei such as the dorsal motor nucleus of the vagus. Also double immunofluorescence for SOD2 and SMI-32 (a marker for motor neurons) reveals that SOD2 immunoreactivity was lost specifically in SMI-32-positive motor neurons and not in SMI-32-negative spinal interneurons (Figs. 1H–J).

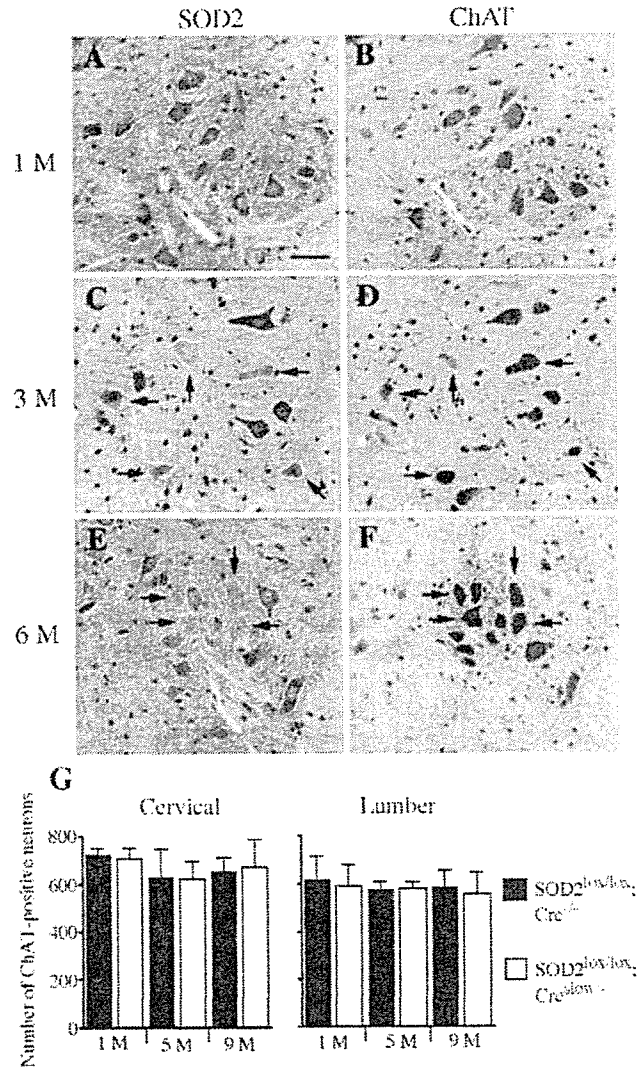

Fig. 2. Detection of SOD2-deficient and ChAT-positive motor neurons in the spinal cord of $SOD2^{lox/lox}$;$Cre^{slow/-}$ mice. Serial paraffin-embedded 5-μm sections of the lumber spinal cord from $SOD2^{lox/lox}$;$Cre^{slow/-}$ mice at 1 month (A, B), 3 months (C, D), or 6 months (E, F) of age were stained with anti-SOD2 (A, C, E) or anti-ChAT (B, D, F) antibodies. Arrows indicate SOD2-negative and ChAT-positive motor neurons. Scale bar = 50 μm. (G) Numbers of spinal cord ChAT-positive motor neurons in $SOD2^{lox/lox}$; $Cre^{slow/-}$ and $SOD2^{lox/lox}$;$Cre^{-/-}$ mice. Numbers were determined from every 5th section for a total of 15 sections. Shown are the means from three mice ± standard deviation (n = 3).

Increased production of $O_2^{\bullet-}$ by mitochondria in $SOD2^{lox/lox}$; $Cre^{slow/-}$ mice

To examine the effect of loss of SOD2 on superoxide production, we compared the spatial production of $O_2^{\bullet-}$ between $SOD2^{lox/lox}$; $Cre^{slow/-}$ and $SOD2^{lox/lox}$; $Cre^{-/-}$ mice by using HEt, a $O_2^{\bullet-}$-specific fluorescent dye (Figs. 1K–N). In the brainstem and spinal cord, punctate ethidium signals in the cytosol reflecting mitochondrial production of $O_2^{\bullet-}$ were detected in motor neurons with large somas, suggesting a relatively high mitochondrial respiratory rate in these

cells under normal physiological conditions. The cytosolic punctate fluorescence of oxidized HEt was more intense in $SOD2^{lox/lox}$; $Cre^{slow/-}$ mice compared to $SOD2^{lox/lox}$;$Cre^{-/-}$ mice in a subset of hypoglossal and spinal cord motor neurons, confirming enhanced production of $O_2^{\bullet -}$ by mitochondria in $SOD2^{lox/lox}$;$Cre^{slow/-}$ mice. On the other hand, this increase in HEt fluorescence was not observed in visceral motor neurons such as the dorsal motor nucleus of the vagus in $SOD2^{lox/lox}$;$Cre^{slow/-}$ mice (data not shown).

Normal neurological and neurochemical profile of $SOD2^{lox/lox}$;$Cre^{slow/-}$ mice

Despite the loss of SOD2 expression and increased superoxide production in motor neurons by 3 months of age (Figs. 2A–F), the number of ChAT-positive motor neurons in the cranial and lumber spinal cord was not significantly different between $SOD2^{lox/lox}$; $Cre^{slow/-}$ and $SOD2^{lox/lox}$;$Cre^{-/-}$ mice at either 5 or 9 months of age (Fig. 2G). Neither overt cell loss nor vacuolar changes in neurons or neuropil were observed as revealed by Nissl-staining of SOD2-negative motor neurons (Figs. 3A–D). Also analyzed was neuronal degeneration by Fluoro-Jade B (Schmued et al., 1997). No Fluoro-Jade B-positive neurons were detected in brain and spinal cord sections from either $SOD2^{lox/lox}$;$Cre^{slow/-}$ or $SOD2^{lox/lox}$; $Cre^{-/-}$ mice (not shown).

As free radicals are a potential source of damage to cellular constituents such as DNA, lipids, and proteins, we evaluated $SOD2^{lox/lox}$;$Cre^{slow/-}$ mice for histochemical signs of oxidative injury and stress. Yet SOD2-deficient motor neurons failed to react with any of the following antibodies: anti-SMI-31 monoclonal antibodies (Sternberger Monoclonals) to phosphorylated neurofilaments which are shown to be accumulated in nerve cell bodies under pathological conditions; a monoclonal antibody against 8-hydroxy-2-deoxyguanosine (8-OHdG; JAICA, Shizuoka, Japan) to oxidative DNA damage; a polyclonal anti-malondialdehyde antibody (MDA; Alpha Diagnostic International, San Antonio, TX) to lipid peroxidation-related MDA-protein adduct; or a monoclonal anti-nitrotyrosine antibody (Upstate Cell Signaling, Lake Placid, NY) to peroxynitrite-mediated protein modification.

A small fraction of SOD1 is reported to reside in the intermembranous space of mitochondria (Okado-Matsumoto and Fridovich, 2001; Mattiazzi et al., 2002; Okado-Matsumoto and Fridovich, 2002) where it may work as an additional line of defense against $O_2^{\bullet -}$. However, immunohistochemical staining showed no obvious compensatory overexpression of SOD1 in the SOD2-deficient motor neurons (Figs. 3E and F). It is still tempting to speculate that an increased amount of SOD1 is accumulated in mitochondria under the SOD2-deficient conditions. A detailed analysis of SOD2 subcellular localization using confocal microscopy or immunoelectron microscopy will be needed to address the possibility.

Next, we analyzed SOD2 expression in ventral halves of the cervical spinal cord micro-dissected from 9-month-old $SOD2^{lox/lox}$; $Cre^{slow/-}$ and $SOD2^{lox/lox}$;$Cre^{-/-}$ mice by immunoblot analysis (Fig. 3G). A significant decrease (30% by densitometry) in SOD2 content was evident in $SOD2^{lox/lox}$;$Cre^{slow/-}$ mice, although again SOD1 expression was unchanged. Even though SOD2 immunoreactivity is most strong in motor neurons in spinal cord sections, the homogenates include mitochondria from various other cell types such as glia and interneurons. Thus, the result shows that SOD2 expression was lost in 30% of the spinal motor neurons at the very least.

Finally, an ultrastructural analysis of mitochondria in motor neurons was undertaken using electron microscopy. Sections of the facial nucleus and spinal cord from 9-month-old $SOD2^{lox/lox}$; $Cre^{slow/-}$ and $SOD2^{lox/lox}$;$Cre^{-/-}$ mice were analyzed. Over 1000 mitochondria in each brain regions were examined, but no degenerative changes such as swelling, disorganization of the cristae or vacuolar formation were observed ($n = 3$ for each genotype; data not shown).

As no obvious phenotype was detected in the cell bodies or organelles of SOD2-deficient motor neurons, we next analyzed the function of axonal processes by looking for muscle denervation and atrophy. Muscle biopsies from $SOD2^{lox/lox}$;$Cre^{slow/-}$ mice revealed

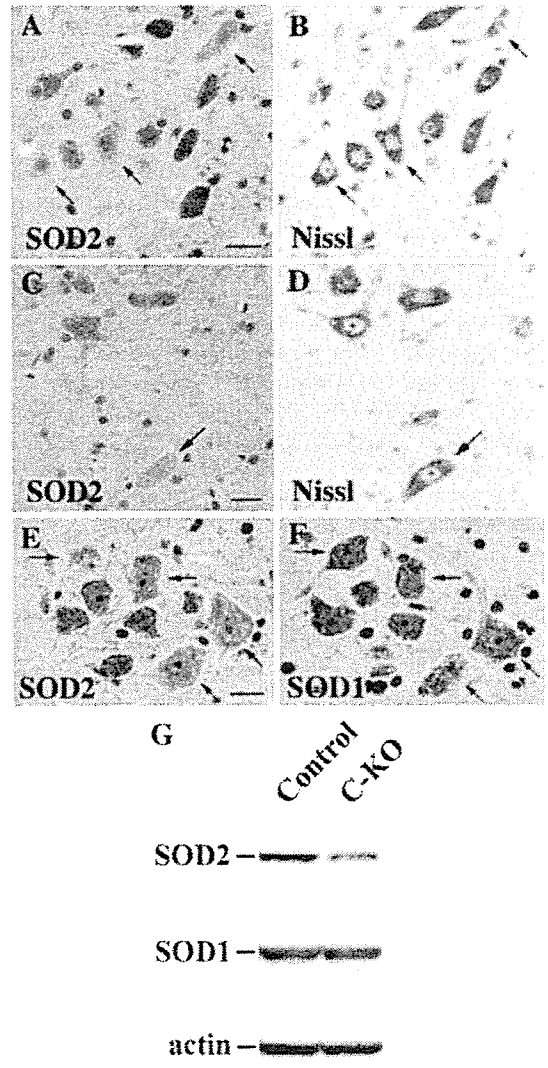

Fig. 3. Morphology of SOD2-deficient motor neurons in 9-month-old $SOD2^{lox/lox}$;$Cre^{slow/-}$ mice. Serial sections from the facial nucleus (A, B) or spinal cord ventral horn (C, D) stained with an anti-SOD2 antibody (A, C) or cresyl violet (Nissl; B, D). No overt morphological changes were seen in the SOD2-defiecent motor neurons (arrows). Serial sections from the hypoglossal nucleus stained with anti-SOD2 (E) or anti-SOD1 (F) antibodies. No difference in the staining pattern or intensity was evident between SOD2-negative (arrows) and SOD2-positive motor neurons. Scale bars = 20 μm. (G) Ventral portions of the spinal cord were micro-dissected from $SOD2^{lox/lox}$;$Cre^{slow/-}$ (C-KO) and $SOD2^{lox/lox}$;$Cre^{-/-}$ (Control) mice. Total homogenates (10 μg) were subjected to immunoblot analysis with polyclonal anti-SOD2 or anti-SOD1 antibodies. Actin content is shown as a loading control.

neither signs of muscle degeneration nor denervation/remodeling of motor axon terminals (Fig. 4). Furthermore, no evidence of reactive gliosis was revealed in $SOD2^{lox/lox}$;$Cre^{slow/-}$ mice by GFAP staining (data not shown), despite its presence in the brainstem motor nuclei of SOD2-null mice (Melov et al., 1998; Lynn et al., 2005).

Motor neuron survival after hypoglossal nerve axotomy is unchanged

Motor neurons in SOD1-deficient mice show an increased vulnerability to facial nerve axotomy despite an otherwise normal phenotype (Reaume et al., 1996). To test whether SOD2-deficient motor neurons are also more vulnerable to nerve injury, we employed unilateral transection of the hypoglossal nerve. Hypoglossal motor neuron survival was then assessed 5 weeks following transection (Fig. 5). Cell number in the axotomized hypoglossal nucleus decreased by approximately 10% compared to the contralateral control side, yet no statistical difference between $SOD2^{lox/lox}$;$Cre^{slow/-}$ and $SOD2^{lox/lox}$;$Cre^{-/-}$ mice was observed (Fig. 5). Furthermore, no difference in the number of SOD2-immunonegative cells was detected in $SOD2^{lox/lox}$;$Cre^{slow/-}$ mice after unilateral axotomy, and similar numbers of atrophic cells were seen in the transected nuclei of $SOD2^{lox/lox}$;$Cre^{slow/-}$ and $SOD2^{lox/lox}$;$Cre^{-/-}$ mice (data not shown).

Motor nerve axon disorganization is accelerated after hypoglossal nerve axotomy

Next, we analyzed the structural stability of the transected hypoglossal axon 2–4 mm distal to the lesion site 2 days postoperation. The distal segment of an injured nerve is known

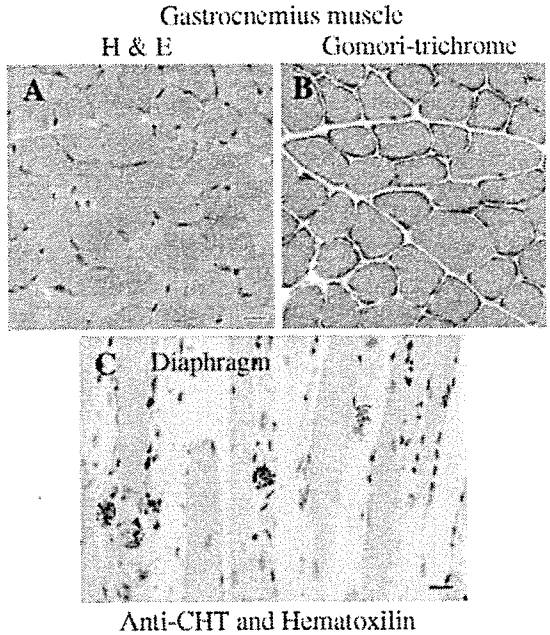

Fig. 4. Absence of muscle atrophy and denervation/remodeling of endplates in $SOD2^{lox/lox}$;$Cre^{slow/-}$ mice. Serial cryosections of gastrocnemius muscle from a 9-month-old $SOD2^{lox/lox}$;$Cre^{slow/-}$ mouse stained with hematoxylin and eosin (A) or Gomori-trichrome (B). Paraffin-embedded sections (5 μm) of diaphragm muscle containing neuromuscular junction from 9-month old $SOD2^{lox/lox}$;$Cre^{slow/-}$ mice stained with an anti-CHT antibody followed by counter-staining with hematoxylin (C). Scale bar = 20 μm.

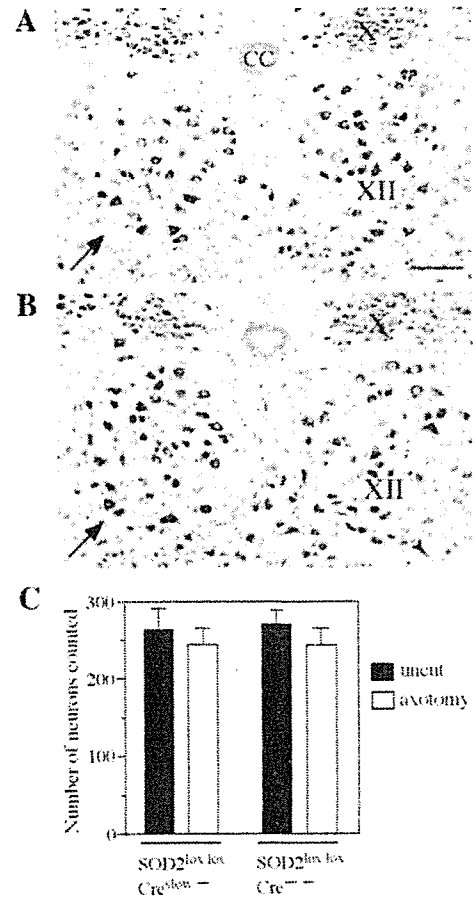

Fig. 5. Nissl-staining of hypoglossal motor neurons 5 weeks after axotomy in $SOD2^{lox/lox}$;$Cre^{slow/-}$ (A) and $SOD2^{lox/lox}$;$Cre^{-/-}$ (B) mice. Arrows indicate the operated side. CC, central canal; X, dorsal motor nucleus of the vagus; XII, hypoglossal nucleus. Scale bar = 100 μm. (C) Number of neurons in hypoglossal nuclei (uncut control or axotomized operated side) from both $SOD2^{lox/lox}$;$Cre^{slow/-}$ and $SOD2^{lox/lox}$;$Cre^{-/-}$ mice ($n = 4$ for each genotype).

to undergo Wallerian degeneration within a few days. In the uncut contralateral nerve, we observed no difference in axon number and diameter between $SOD2^{lox/lox}$;$Cre^{slow/-}$ and $SOD2^{lox/lox}$;$Cre^{-/-}$ mice. However, $SOD2^{lox/lox}$;$Cre^{slow/-}$ axons did show an accelerated degeneration after nerve injury. When compared with $SOD2^{lox/lox}$;$Cre^{-/-}$ mice both cytoskeletal protein stability as revealed by Western blot and axon structure as revealed by histological analysis were significantly altered (Fig. 6).

Discussion

The present study demonstrates for the first time that SOD2 is not required for postnatal motor neurons survival and further reveals that motor neurons are, in fact, quite resistant to mitochondrial generated $O_2^{\bullet-}$ in vivo. In the absence of SOD enzymatic activity, $O_2^{\bullet-}$ is relatively stable. Other antioxidants such as glutathione, ascorbate and tocopherols are relatively inefficient in removing superoxide radicals, and spontaneous dismutation occurs only very slowly. Because a portion of enzymatically active SOD1 is detected in the mitochondrial intermembranous space (Okado-Matsumoto and Fridovich, 2001; Mattiazzi

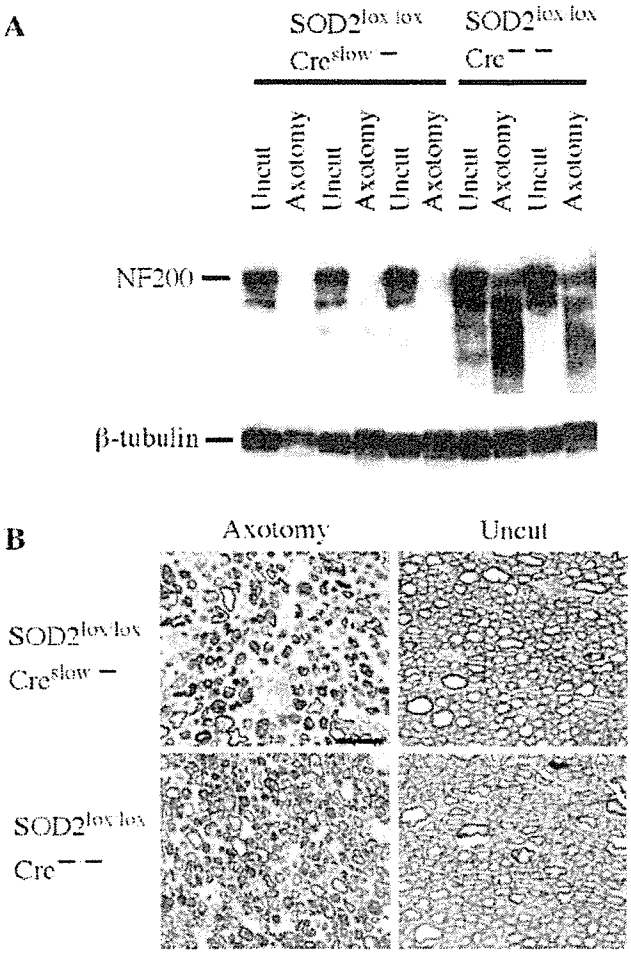

Fig. 6. Accelerated axonal disorganization in $SOD2^{lox/lox}$;$Cre^{slow/-}$ mice after motor nerve injury. (A) Western blot of 200-kDa neurofilament protein (NF-200) demonstrating the extent of degeneration 2 days after nerve transection in the distal transected hypoglossal nerve (Axotomy) or corresponding contralateral uncut nerve (Uncut). The blot was reprobed with control monoclonal antibody (β-tub 2.1) against β-tubulin. Samples from three $SOD2^{lox/lox}$;$Cre^{slow/-}$ and two $SOD2^{lox/lox}$;$Cre^{-/-}$ control mice are shown. (B) Representative toluidine blue-stained sections of hypoglossal nerves 2–4 mm distal to the lesion site 2 days after transection or corresponding contralateral uninjured nerve. Scale bar = 20 μm.

et al., 2002; Okado-Matsumoto and Fridovich, 2002), we speculate that, although the physiological functions of SOD1 in the mitochondria are not fully understood, some SOD2 function is compensated by SOD1 potentially by removing $O_2^{\bullet-}$ generated from complex III (Han et al., 2001). And although we did not detect SOD1 upregulation in SOD2-deficient motor neurons (Figs. 3E and F), endogenous levels of mitochondrial SOD1 may be sufficient to prevent both $O_2^{\bullet-}$-induced mitochondrial injury and $O_2^{\bullet-}$ release from mitochondria to cytosol. The physiological role and possible compensation of SOD2 loss by SOD1 can be addressed in future studies by crossing $SOD2^{lox/lox}$;$Cre^{slow/-}$ mice to a SOD1-null background.

Motor neurons in the SOD1-deficient mice are vulnerable to axotomy-induced oxidative burden (Reaume et al., 1996). In the present study, we have analyzed the effect of nerve transection on motor neurons lacking SOD2 expression. We demonstrate here that neuronal survival after axotomy is not affected, but that disorganization of distal nerve axons is accelerated in the SOD2-deficient motor neurons. Thus, loss of SOD2 function is insufficient to kill transected motor neurons but does trigger more rapid motor axon degeneration after nerve injury. Although we do not yet understand the mechanism underlying the observed accelerated disorganization, we speculate that abnormal Ca^{2-} handling in SOD2-deficient mitochondria results in lowered Ca^{2+}-buffering activity specifically in lesioned distal axons while leaving the cell bodies unaffected. Interestingly, neurofilament proteins are known to be particularly susceptible tyrosine nitration and lysine oxidation (Beckman et al., 1993). Our present study thus implicates a previously unrecognized link between mitochondrial oxidative stress and axonal vulnerability to injury.

ALS is a fatal adult-onset neurodegenerative disease characterized by the selective loss of upper and lower motor neurons. Although its cause is not fully understood, mutations in the SOD1 gene cause a familial form of ALS, and recent studies show involvement of mitochondrial dysfunction and oxidative damage in ALS pathogenesis (Andersen, 2004; Bendotti and Carri, 2004; Bruijn et al., 2004; Xu et al., 2004). In animal models, mitochondrial abnormalities were seen in motor neurons of mice or rats expressing the SOD1 mutations $SOD1^{G93A}$ (Dal Canto and Gurney, 1994; Jaarsma et al., 2001; Howland et al., 2002) and $SOD1^{G37R}$ (Wong et al., 1995), but similar pathology was not detected in motor neurons expressing other types of mutant SOD1 (Bruijn et al., 1997; Nagai et al., 2001). Furthermore, Andreassen et al. (2000) reported that heterozygous loss of SOD2 exacerbates disease in mutant SOD1 transgenic mice. Recent studies show that mutant SOD1, rather than abrogating function, acquires a toxic function and that mutant SOD1 expression is required in both neurons and glia cells to induce motor neuron degeneration (Gong et al., 2000; Pramatarova et al., 2001; Lino et al., 2002; Clement et al., 2003). The present study also is consistent with a possible importance of interplay between neurons and glia cells in motor neuron survival.

In an ALS mouse model, expression of the neuronal isoform of nitric oxide synthase (nNOS) is increased in astrocytes surrounding motor neurons in the spinal cord and brainstem (Cha et al., 1998). Also increased nitrotyrosine labeling in motor neurons and in the ventral horn has been reported in ALS and mutant SOD1-expressing mouse models (Abe et al., 1995; Beal et al., 1997; Ferrante et al., 1997; Cha et al., 2000). In the present study, we did not find any nitrotyrosine immuno-positive cells in the brain and spinal cord of 9-month-old $SOD2^{lox/lox}$;$Cre^{slow/-}$ mice. Furthermore, neither signs of reactive gliosis (GFAP-IR) nor peroxynitrite-mediated oxidative damage (nitrotyrosine-IR) in astrocytes surrounding SOD2-deficient motor neurons were evident. We speculate that elevated levels of $O_2^{\bullet-}$ in motor neurons is not by itself enough to trigger chronic cell injury, but NO produced from neighboring astrocytes resulting in peroxynitrite production may be a further requirement to trigger ROS-induced toxicity.

Axonal disorganization and reduced slow axonal transport are well-known hallmarks of ALS. Although our present results indicate that loss of SOD2 function is not by itself sufficient to kill motor neurons in vivo, it does modify axonal susceptibility to nerve injury. Recently Vande Velde et al. (2004) reported that Wld^S protein, the dominant neuroprotective factor that markedly delays Wallerian axonal degeneration after nerve injury, does not prevent SOD1-mediated motor neuron loss when introduced the Wld^S mutation into the $SOD1^{G37R}$ or $SOD1^{G85R}$ ALS mouse models. These results show that inhibiting axonal degeneration is not

effective to ameliorate ALS pathogenesis induced by the mutant SOD1 protein.

Although the precise pathologic role of $O_2^{\bullet -}$ in motor neuron degeneration remains to be fully clarified, the present study is consistent with the possible involvement of nonneuronal cells in mitochondrial-derived, superoxide-induced injury in motor neurons. Thus, a rational therapeutic strategy that delivers antioxidants to surrounding astrocytes or microglia may significantly help motor neurons survive oxidative stress.

Acknowledgments

The authors thank Drs. K. Amano and K. Yamakawa (RIKEN Brain Science Institute) for FISH analysis of VAChT-Cre.Slow mice; Drs. K. Endo and M. Ichikawa (Tokyo Metropolitan Institute for Neuroscience; TMIN) for valuable advice on electron microscopy; Drs. K. Kohyama, Y. Matsumoto, and T. Uchihara (TMIN) for muscle biopsy; and Dr. S. E. Craven for critical reading of the manuscript. This work was supported by grants from the Ministry of Education, Culture, Sports, Science and Technology, Japan, and from the Japanese Ministry of Health, Labor and Welfare, Research on Psychiatric and Neurological Diseases and Mental Health.

References

Abe, K., Pan, L.-H., Watanabe, M., Kato, T., Itoyama, Y., 1995. Induction of nitrotyrosine-like immunoreactivity in the lower motor neuron of amyotrophic lateral sclerosis. Neurosci. Lett. 199, 152–154.

Andersen, J.K., 2004. Oxidative stress in neurodegeneration: cause or consequence? Nat. Med. 10, S18–S25 (Suppl.).

Andreassen, O.A., Ferrante, R.J., Klivenyi, P., Klein, A.M., Shinobu, L.A., Epstein, C.J., Beal, M.F., 2000. Partial deficiency of manganese superoxide dismutase exacerbates a transgenic mouse model of amyotrophic lateral sclerosis. Ann. Neurol. 47, 447–455.

Beal, M.F., 1996. Mitochondria, free radicals, and neurodegeneration. Curr. Opin. Neurobiol. 6, 661–666.

Beal, M.F., Ferrante, R.J., Browne, S.E., Matthews, R.T., Kowall, N.W., Brown Jr., R.H., 1997. Increased 3-nitrotyrosine in both sporadic and familial amyotrophic lateral sclerosis. Ann. Neurol. 42, 644–654.

Beckman, J.S., Carson, M., Smith, C.D., Koppenol, W.H., 1993. ALS, SOD and peroxynitrite. Nature 364, 584.

Bendotti, C., Carri, M.T., 2004. Lessons from models of SOD1-linked familial ALS. Trends Mol. Med. 10, 393–400.

Bindokas, V.P., Jordan, J., Lee, C.C., Miller, R.J., 1996. Superoxide production in rat hippocampal neurons: selective imaging with hydroethidine. J. Neurosci. 16, 1324–1336.

Bruijn, L.I., Becher, M.W., Lee, M.K., Anderson, K.L., Jenkins, N.A., Copeland, N.G., Sisodia, S.S., Rothstein, J.D., Borchelt, D.R., Price, D.L., Cleveland, D.W., 1997. ALS-linked SOD1 mutant G85R mediates damage to astrocytes and promotes rapidly progressive disease with SOD1-containing inclusions. Neuron 18, 327–338.

Bruijn, L.I., Miller, T.M., Cleveland, D.W., 2004. Unraveling the mechanisms involved in motor neuron degeneration in ALS. Annu. Rev. Neurosci. 27, 723–749.

Cha, C.I., Kim, J.-M., Shin, D.H., Kim, Y.S., Kim, J., Gurney, M.E., Lee, K.W., 1998. Reactive astrocytes express nitric oxide synthase in the spinal cord of transgenic mice expressing a human Cu/Zn SOD mutation. NeuroReport 9, 1503–1506.

Cha, C.I., Chung, Y.H., Shin, C.-M., Shin, D.H., Kim, Y.S., Gurney, M.E., Lee, K.W., 2000. Immunocytochemical study on the distribution of nitrotyrosine in the brain of the transgenic mice expressing a human Cu/Zn SOD mutation. Brain Res. 853, 156–161.

Clement, A.M., Nguyen, M.D., Roberts, E.A., Garcia, M.L., Boillee, S., Rule, M., McMahon, A.P., Doucette, W., Siwek, D., Ferrante, R.J., Brown Jr., R.H., Julien, J.-P., Goldstein, L.S.B., Cleveland, D.W., 2003. Wild-type nonneuronal cells extend survival of SOD1 mutant motor neurons in ALS mice. Science 302, 113–117.

Dal Canto, MC., Gurney, M.E., 1994. Development of central nervous system pathology in a murine transgenic model of human amyotrophic lateral sclerosis. Am. J. Pathol. 145, 1271–1279.

Ferrante, R.J., Shinobu, L.A., Schulz, R.T., Matthews, R.T., Thomas, C.E., Kowall, N.W., Gurney, M.E., Beal, M.F., 1997. Increased 3-nitrotyrosine and oxidative damage in mice with a human copper/zinc superoxide dismutase mutation. Ann. Neurol. 42, 326–334.

Gong, Y.H., Parsadanian, A.S., Andreeva, A., Snider, W.D., Elliott, J.L., 2000. Restricted expression of G86R Cu/Zn superoxide dismutase in astrocytes results in astrocytosis but does not cause motoneuron degeneration. J. Neurosci. 20, 660–665.

Han, D., Williams, E., Cadenas, E., 2001. Mitochondrial respiratory chain-dependent generation of superoxide anion and its release into the intermembrane space. Biochem. J. 353, 411–416.

Hjalmarsson, K., Marklund, S.L., Engstrom, A., Edlund, T., 1987. Isolation and sequence of complementary DNA encoding human extracellular superoxide dismutase. Proc. Natl. Acad. Sci. U. S. A. 84, 6340–6344.

Howland, D.S., Liu, J., She, Y., Goad, B., Maragakis, N.J., Kim, B., Erickson, J., Kulik, J., DeVito, L., Psaltis, G., DeGennaro, L.J., Cleveland, D.W., Rothstein, J.D., 2002. Focal loss of the glutamate transporter EAAT2 in a transgenic rat model of SOD1 mutant-mediated amyotrophic lateral sclerosis (ALS). Proc. Natl. Acad. Sci. U. S. A. 99, 1604–1609.

Huang, T.T., Carlson, E.J., Kozy, H.M., Mantha, S., Goodman, S.I., Ursell, P.C., Epstein, C.J., 2001. Genetic modification of prenatal lethality and dilated cardiomyopathy in Mn superoxide dismutase mutant mice. Free Radical Biol. Med. 31, 1101–1110.

Ichikawa, T., Ajiki, K., Matsuura, J., Misawa, H., 1997. Localization of two cholinergic markers, choline acetyltransferase and vesicular acetylcholine transporter in the central nervous system of the rat: in situ hybridization histochemistry and immunohistochemistry. J. Chem. Neuroanat. 13, 23–39.

Ikegami, T., Suzuki, Y., Shimizu, T., Isono, K., Koseki, H., Shirasawa, T., 2002. Model mice for tissue-specific deletion of the manganese superoxide dismutase (MnSOD) gene. Biochem. Biophys. Res. Commun. 296, 729–736.

Jaarsma, D., Rognoni, F., van Duijn, W., Verspaget, H.W., Haasdijk, E.D., Holstege, J.C., 2001. CuZn superoxide dismutase (SOD1) accumulates in vacuolated mitochondria in transgenic mice expressing amyotrophic lateral sclerosis-linked SOD1 mutations. Acta Neuropathol. (Berlin) 102, 239–305.

Lebovitz, R.M., Zhang, H., Vogel, H., Cartwright Jr., J., Dionne, L., Lu, N., Huang, S., Matzuk, M.M., 1996. Neurodegeneration, myocardial injury, and perinatal death in mitochondrial superoxide dismutase-deficient mice. Proc. Natl. Acad. Sci. U. S. A. 93, 9782–9787.

Li, Y., Huang, T.-T., Carlson, E.J., Melov, S., Ursell, P.C., Olson, J.L., Noble, L.J., Yoshimura, M.P., Berger, C., Chan, P.H., Wallace, D.C., Epstein, C.J., 1995. Dilated cardiomyopathy and neonatal lethality in mutant mice lacking manganese superoxide dismutase. Nat. Genet. 11, 376–381.

Lino, M.M., Schneider, C., Caroni, P., 2002. Accumulation of SOD1 mutants in postnatal motoneurons does not cause motoneuron pathology or motoneuron disease. J. Neurosci. 22, 4825–4832.

Lynn, S., Huang, E.J., Elchuri, S., Naeemuddin, M., Nishinaka, Y., Yodoi, J., Ferriero, D., Epstein, M., Huang, C.J., 2005. Selective neuronal vulnerability and inadequate stress response in superoxide dismutase mutant mice. Free Radical Biol. Med. 38, 817–828.

Mack, T.G.A., Reiner, M., Beirowski, B., Mi, W., Emanuelli, M., Wagner, D., Thomson, D., Gillingwater, T., Court, F., Conforti, L., Fernando, F.S., Tarlton, A., Andressen, C., Addicks, K., Magni, G., Ribchester,

R.R., Perry, V.H., Coleman, M.P., 2001. Wallerian degeneration of injured axons and synapses is delayed by a Ube4b/Nmnat chimeric gene. Nat. Neurosci. 4, 1199–1206.

Marklund, S.L., 1982. Human copper-containing superoxide dismutase of high molecular weight. Proc. Natl. Acad. Sci. U. S. A. 79, 7634–7638.

Mattiazzi, M., D'Aurelio, M., Gajewski, C.D., Martushova, K., Kiaei, M., Beal, M.F., Manfredi, G., 2002. Mutated human SOD1 causes dysfunction of oxidative phosphorylation in mitochondria of transgenic mice. J. Biol. Chem. 277, 29626–29633.

McCord, J.M., Fridovich, I., 1969. The utility of superoxide dismutase in studying free radical reaction: I. Radicals generated by the interaction of sulfite, dimetyl sulfoxide, and oxygen. J. Biol. Chem. 244, 6056–6063.

Melov, S., Schneider, J.A., Day, B.J., Hinerfeld, D., Coskun, P., Mirra, S.S., Crapo, J.D., Wallace, D.C., 1998. A novel neurological phenotype in mice lacking mitochondrial manganese superoxide dismutase. Nat. Genet. 18, 159–163.

Misawa, H., Nakata, K., Matsuura, J., Nagao, M., Okuda, T., Haga, T., 2001. Distribution of the high-affinity choline transporter in the central nervous system of the rat. Neuroscience 105, 87–98.

Misawa, H., Nakata, K., Toda, K., Matsuura, J., Oda, Y., Inoue, H., Taneno, M., Takahashi, R., 2003. VAChT-Cre.Fast and VAChT-Cre.Slow: postnatal expression of Cre recombinase in somatomotor neurons with different onset. Genesis 37, 44–50.

Murakami, K., Kondo, T., Kawase, M., Li, Y., Sato, S., Chen, S.F., Chan, P.H., 1998. Mitochondrial susceptibility to oxidative stress exacerbates cerebral infarction that follows permanent focal cerebral ischemia in mutant mice with manganese superoxide dismutase deficiency. J. Neurosci. 18, 205–213.

Nagai, M., Aoki, M., Miyoshi, I., Kato, M., Pasinelli, P., Kasai, N., Brown Jr., R.H., Itoyama, Y., 2001. Rats expressing human cytosolic copper-zinc superoxide dismutase transgenes with amyotrophic lateral sclerosis: associated mutations develop motor neuron disease. J. Neurosci. 21, 9246–9254.

Okado-Matsumoto, A., Fridovich, I., 2001. Subcellular distribution of superoxide dismutases (SOD) in rat liver. J. Biol. Chem. 276, 38388–38393.

Okado-Matsumoto, A., Fridovich, I., 2002. Amyotrophic lateral sclerosis: a proposed mechanism. Proc. Natl. Acad. Sci. U. S. A. 99, 9010–9014.

Pramatarova, A., Laganiere, J., Roussel, J., Brisbois, K., Rouleau, G.A., 2001. Neuron-specific expression of mutant superoxide dismutase 1 in transgenic mice does not lead to motor impairment. J. Neurosci. 21, 3369–3374.

Reaume, A.G., Elliott, J.L., Hoffman, E.K., Kowall, N.W., Ferrante, R.J., Siwek, D.F., Wilcox, H.M., Flood, D.G., Beal, M.F., Brown Jr., R.H., Scott, R.W., Snider, W.D., 1996. Motor neurons in Cu/Zn superoxide dismutase-deficient mice develop normally but exhibit enhanced cell death after axonal injury. Nat. Genet. 13, 43–47.

Schmued, L.C., Albertson, C., Slikker Jr., W., 1997. Fluoro-Jade: a novel fluorochrome for the sensitive and reliable histochemical localization of neuronal degeneration. Brain Res. 751, 37–46.

Vande Velde, C., Garcia, M.L., Yin, X., Trapp, B.D., Cleveland, D.W., 2004. The neuroprotective factor Wld^{s} does not attenuate mutant SOD1-mediated motor neuron disease. Neuromol. Med. 5, 193–203.

Weisiger, R.A., Fridovich, I., 1973. Mitochondrial superoxide dismutase: site of synthesis and intramitochondrial localization. J. Biol. Chem. 248, 4793–4796.

Wong, P.C., Pardo, C.A., Borchelt, D.R., Lee, M.K., Copeland, N.G., Jenkins, N.A., Sisodia, S.S., Cleveland, D.W., Price, D.L., 1995. An adverse property of a familial ALS-linked SOD1 mutation causes motor neuron disease characterized by vacuolar degeneration of mitochondria. Neuron 14, 1105–1116.

Xu, Z., Jung, C., Higgins, C., Levine, J., Kong, J., 2004. Mitochondrial degeneration in amyotrophic lateral sclerosis. J. Bioenerg. Biomembr. 36, 395–399.

ELSEVIER

Journal of the Neurological Sciences 247 (2006) 109 - 111

Journal of the Neurological Sciences

www.elsevier.com/locate/jns

Short communication

Epileptic polyopia with right temporal lobe epilepsy as studied by FDG-PET and MRI: A case report

Takahiro Mitsueda-Ono [a], Akio Ikeda [a,*], Eri Noguchi [a], Shigetoshi Takaya [b], Hidenao Fukuyama [b], Shun Shimohama [a], Ryosuke Takahashi [a]

[a] *Department of Neurology, Kyoto University Hospital, 54 Shogoin-Kawaharacho, Sakyo-ku, Kyoto 606-8507, Japan*
[b] *Human Brain Research Center, Kyoto University School of Medicine, Japan*

Received 30 December 2005; received in revised form 14 April 2006; accepted 18 April 2006
Available online 21 June 2006

Abstract

Polyopia is one of rare, visual hallucinations. A 61-year-old man suffered from daily episodes of polyopia and generalized convulsions, and he was diagnosed as right temporal lobe epilepsy. MRI revealed right amygdalar swelling. FDG-PET showed hypometabolism in the right anterior temporal and the mesial occipital areas. Polyopia is thought to be caused by dysfunction of updating process of visual information in the visual association cortices. It was most likely that, in this patient, both mesial temporal and ipsilateral occipital areas were responsible for manifesting epileptic polyopia, as ictal onset zone and symptomatogenic zone, respectively.

Keywords: Polyopia; Partial epilepsy; Amygdala; FDG-PET

1. Introduction

Polyopia is one of complex visual hallucinations, manifesting appearance of plural images as erroneous visual perceptions even after the object has left out of visual field. On the other hand, palinopsia is also a kind of visual hallucinations, appearing plenty of the same images while watching one object [1]. Since this report, it was frequently reported referring to several neurological disorders, but it seems to involve temporo-occipital area commonly.

On the other hand, human "amygdalar epilepsy" is not established yet [2]. Amongst a series of 174 cases with intractable temporal lobe epilepsy (TLE) confirmed by video EEG monitoring, amygdalar enlargement was observed in seven patients (4%) [3].

This is the first report that mentioned amygdalar enlargement and interictal PET study in epilepsy patients having polyopia. It may suggest that amygdala is also involved in manifesting polyopia as the ictal onset zone, but not necessarily as the symptomatogenic zone.

2. Case report

A 61-year-old right-handed man, without history of febrile convulsions, any developmental problems or head injury, was admitted because he had very frequent episodes of seeing "multiple, identical images previously seen" (called as polyopia as explained below) that were overlapped on his real vision mainly on the left side. He had several episodes of generalized convulsions with tongue bite since the age of 47 years, and he was free from generalized convulsions in the last 14 years, but the current type of visual symptoms started since age 60 years. Frequency of the current attacks has increased from once per 2 or 3 days to several times per day.

The polyopia episodes were elaborated as follows. He saw multiple, same persons who had been seen just before;

Abbreviations: EEG, electroencephalography; MRI, magnetic resonance image; FDG, fluorodeoxyglicose; PET, positron emission computed tomography; TLE, temporal lobe epilepsy; AVM, artery venous malformation; FLAIR, fluid-attenuated inversion recovery.

* Corresponding author. Tel.: +81 75 751 3772; fax: +81 75 751 9416.
E-mail address: akio@kuhp.kyoto-u.ac.jp (A. Ikeda).

0022-510X/$ - see front matter © 2006 Elsevier B.V. All rights reserved.
doi:10.1016/j.jns.2006.04.010

he had an episode while playing an aerobic dance and saw multiple same persons in front of him in a row who were actually playing side to him. On the other occasions, he saw some people around him whom he could not identify, and the experienced scene was accompanied. He felt as if he was moving along these people in the scene (Fig. 1), followed by ascending sensation of numbness on his trunk bilaterally. Each episode lasted about 10 s, and initially he was aware and he thought that he did not lose his consciousness. One of the authors witnessed the episode when he showed incoherent vocalization, oral and hand automatisms, no responsiveness and test words given during the episode were not remembered, being consistent with simple partial seizures followed by complex partial seizures. Once the visual symptoms started, he felt angry against and wanted to quit or overcome the episodes; otherwise, other emotional symptoms were not accompanied.

He has no family history of neurological diseases. General and neurological examinations revealed no abnormality in the interictal period. Interictal EEG showed intermittent irregular slow (2.5 to 3 Hz) activity in the right fronto-temporal area, and several sharp transients in the right midtemporal area once per several minutes. Ictal EEG was not recorded.

The right amygdala increased in size on MRI (Fig. 2a and b), and there were no gadolinium-enhanced lesions. The intensity in FLAIR images was not increased. Neither hippocampal atrophy nor sclerosis was detected on both sides. In FDG-PET study, there was regional glucose hypometabolism in the right temporal and in the caudal part along the calcarine fissure in the right medial occipital area (Fig. 3). As compared with healthy subjects by using SPM, regional glucose hypometabolism was significant in the right temporo-occipital area.

All neuropsychological examinations resulted in normal limits as follows: Wechsler Memory Scale: verbal 96, visual 117, general 103, attention 106, delay 96; Western Aphasia Battery: AQ 100, CQ 99.4; Raven's colored progressive matrices test: 32/37; Boston Naming Test: 48/60; Wechsler Adult Intelligence Scale-Revised: verbal IQ 131, performance IQ 136, total IQ 136.

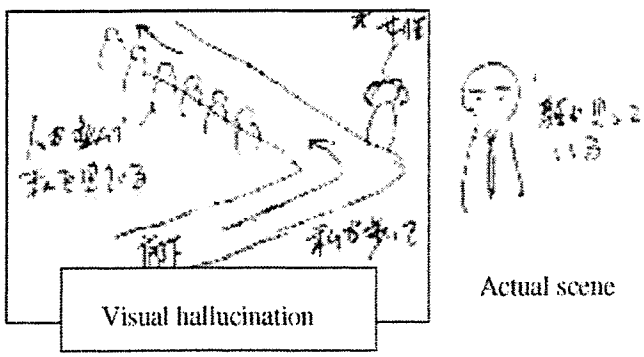

Fig. 1. One example of the polyopia drawn by the patient. While facing the doctor to whom he was talking, suddenly he felt as if he was walking along the corridor. Besides, he saw a row of the same unidentified persons and an unidentified woman who he just met before along the corridor. This visual hallucination appeared in the left visual field.

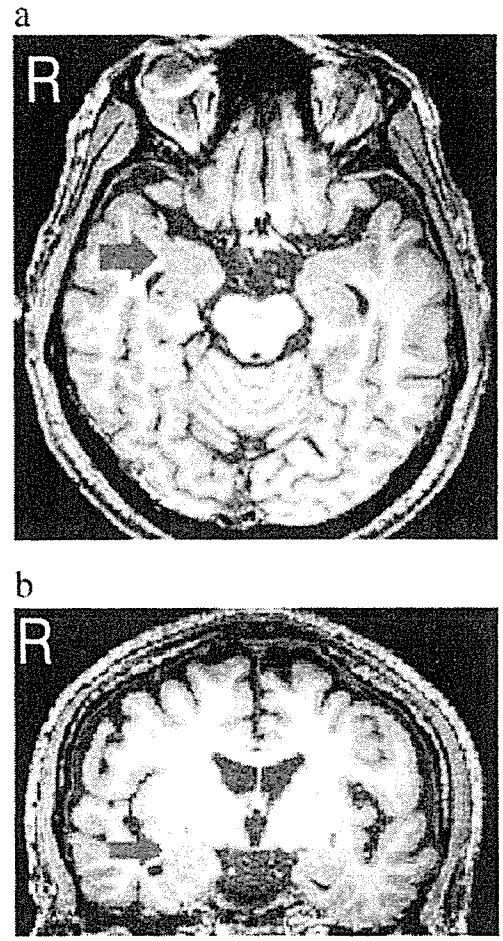

Fig. 2. T1-weighed MRI images. Right amygdalar enlargement was found in the axial (a) and the coronal (b) images. Arrow shows the enlarged amygdala.

We diagnosed him as right TLE based on ictal semiology, EEG, MRI and FDG-PET, and thus carbamazepine was started. It was gradually increased up to 300 mg/day, and his ictal symptoms have completely stopped.

3. Discussion

There were several reports that mentioned polyopia as seen in the present patient until now; however, it was rarely reported. According to those reports, it was observed in patients with cerebral infarction [1], head trauma [4], AVM [5], multiple sclerosis [6], non-ketoacidotic hyperglycemia [7], Creutzfeldt-Jakob disease [8] and migraine [9]. In case of partial epilepsy, occipitotemporal region or hippocampus was responsible [10].

From stimulation study, simple visual hallucination (e.g., light or scotoma) occurred by the stimulation of area 18 or 19 [11]. Lateral temporal lobe correlates with playback of sensory input. Stimulation of this region reminded patients of previously experienced scene [11].

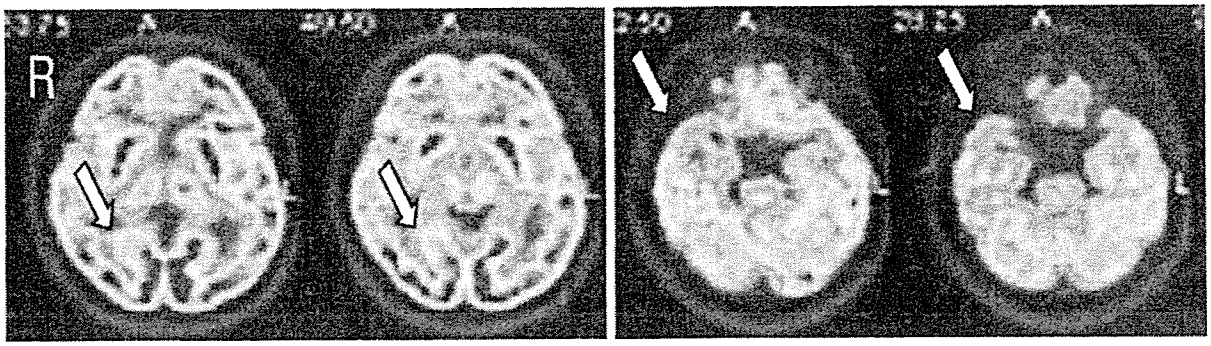

Fig. 3. PET study revealed hypometabolism in the right temporal lobe and right mesial occipital area (as shown by arrows).

In order to constitute polyopia, dysfunction of updating ongoing spatial perception in response to the circumstances would be necessary. It could occur by the impairment of not primary visual cortex but lateral temporal lobe, which correlates to record and accumulate visual perception. The responsible area for polyopia has remained unsolved; however, the abnormal input to the visual association cortex located in the temporo-occipito-parietal area could be one of the causes [12].

In the present patient, both right anterior temporal and mesial occipital areas were involved according to FDG-PET study. Hypometabolic brain areas as revealed by FDG-PET indicate not only epileptogenic but also symptomatogenic brain regions [13]. Hence, these two regions are involved as either symptomatogenic or epileptogenic zone. Right anterior temporal area (frequent interictal spikes in interictal EEG), especially the swollen right amygdala, most likely plays an important role as epileptogenic zone.

Amygdalar enlargement is a distinct entity from mesial temporal sclerosis. When we consider medial temporal lobe epilepsy, it is necessary to pay attention to amygdalar abnormality. Abnormal EEG discharges with amygdalar enlargement that acts as epileptogenic zone can lead to ipsilateral occipital area as symptomatogenic zone. This finding also suggests the connection between amygdala and occipital lobe. Additionally, it is also noteworthy that polyopia can manifest even in patients with TLE since an epileptogenic zone could be distant from the symptomatogenic zone of polyopia.

Acknowledgement

This study was supported by the Research Grant for the Treatment of Intractable Epilepsy (16-1) from the Japan Ministry of Health, Labor and Welfare, and a Scientific Research Grant (C2) 18590935 from the Japan Society for Promotion of Sciences.

References

[1] Critchley M. Types of visual preservation: "palinopsia" and "illusory visual spread". Brain 1951;74:267–99.
[2] Wieser HG. Mesial temporal lobe epilepsy versus amygdalar epilepsy: late seizure recurrence after initially successful amygdalotomy and regained seizure control following hippocampectomy. Epileptic Disord 2000;2:141–51.
[3] Bower SPC, Vorgin SJ, Morris K, Cox I, Murphy M, Kilpatrick CJ, et al. Amygdala volumetry in "imaging-negative" temporal lobe epilepsy. J Neurol Neurosurg Psychiatry 2003;74:1245–9.
[4] Kinsbourne M. Warrington EK. A study of visual preservation. J Neurol Neurosurg Psychiatry 1963;26:468–75.
[5] Jacobs L. Visual allesthesia. Neurology 1980;30:1059–63.
[6] Jacome DE. Palinopsia and bitemporal visual extinction on fixation. Ann Ophthalmol 1985;17:251–2.
[7] Johnson SF, Loge RV. Palinopsia due to nonketotic hyperglycemia. West J Med 1988;148:331–2.
[8] Purvin V, Bomin J, Goodman J. Palinopsia as a presenting manifestation of Creutzfeldt-Jacob disease. J Clin Neuroophthalmol 1989;9:242–8.
[9] Klee A, Willanger R. Disturbances of visual perception in migraine: review of the literature and a report of eight cases. Acta Neurol Scand 1966;42:400–14.
[10] Christian GB, Felix OB, Horst U, Johannes S, Martin K, Christian EE. Localizing value of epileptic visual auras. Brain 2000;123:244–53.
[11] Penfield W, Perot P. The brain's record of auditory and visual experience. Brain 1963;86:596–696.
[12] Okada K, Akamatsu N, Hashimoto T, Uozumi T, Tsuji S. A case of right mesial temporal lobe epilepsy accompanied with ictal polyopsia. Clin Neurol 2004;44:39–42 [Only abstract written in English].
[13] Schlaug G, Antke C, Holthausen H, Arnold S, Ebner A, Tuxhorn I, et al. Ictal motor signs and interictal regional cerebral hypometabolism. Neurology 1997;49:341–50.

ELSEVIER

Clinical Neurophysiology 117 (2006) 1481–1486

www.elsevier.com/locate/clinph

Generators and temporal succession of giant somatosensory evoked potentials in cortical reflex myoclonus: Epicortical recording from sensorimotor cortex

Takefumi Hitomi [a], Akio Ikeda [a,*], Riki Matsumoto [a], Masako Kinoshita [a], Junya Taki [b], Keiko Usui [c], Nobuhiro Mikuni [b], Takashi Nagamine [c], Nobuo Hashimoto [b], Hiroshi Shibasaki [d], Ryosuke Takahashi [a]

[a] *Department of Neurology, Kyoto University Graduate School of Medicine, Kyoto, Japan*
[b] *Department of Neurosurgery, Kyoto University Graduate School of Medicine, Kyoto, Japan*
[c] *Department of Brain Pathophysiology, Human Brain Research Center, Kyoto University Graduate School of Medicine, Kyoto, Japan*
[d] *Takeda General Hospital, Kyoto, Japan*

Accepted 29 March 2006

Abstract

Objective: To clarify the generator mechanism of giant somatosensory evoked potentials (giant SEPs) and the hyperexcitability of primary somatosensory and motor cortices (SI and MI).

Methods: In a patient with intractable focal seizures manifesting cortical reflex myoclonus of the left foot, giant SEPs to left tibial nerve stimulation were epicortically recorded as a part of presurgical evaluation with subdural electrodes.

Results: In the single pulse SEPs, enlarged P1–N1 components were observed at the foot area of the SI and MI (86.5–258.8 μV, respectively), and the peak latencies were always shorter at SI than at MI by 6 ms. Similar findings were obtained for peroneal and sural nerve stimulation. In the paired pulse SEPs, the second response was less suppressed, as compared to other interstimulus intervals (ISIs), with ISIs of 40 and 200 ms both at SI and MI.

Conclusions: In this particular patient, cortical hyperexcitability to somatosensory stimuli seems to originate from SI but subsequently both SI and MI are responsible for the generation of giant SEPs and cortical reflex myoclonus.

Significance: Somatosensory and primary motor cortices both generated enhanced early cortical components of SEPs, most likely by enhancing the latter by the former.

Keywords: Giant somatosensory evoked potential (giant SEP); Cortical reflex myoclonus; Primary somatosensory cortex (SI); Primary motor cortex (MI)

1. Introduction

Extremely enlarged cortical components of somatosensory evoked potentials (giant SEPs) are observed in the majority of patients with cortical reflex myoclonus. The giant SEPs are considered to represent the degree of cortical hyperexcitability of the primary sensorimotor cortices (SMI) in response to somatosensory stimuli (Shibasaki et al., 1985), and are considered to result from pathological enhancement of certain early components of normal SEPs (Ikeda et al., 1995; Kakigi and Shibasaki, 1987a; Shibasaki

Abbreviations: SEP, somatosensory evoked potential; SMI, primary sensorimotor cortices; SI, primary somatosensory cortex; MI, primary motor cortex; ISI, interstimulus interval; SEP-R, SEP recovery function; ECoG, electrocorticogram; MEG, magnetoencephalography; SEF, somatosensory evoked magnetic field.

* Corresponding author. Address: Department of Neurology, Kyoto University Hospital, 54 Shogoin-Kawaharacho, Sakyo-ku, Kyoto 606-8507, Japan. Tel.: +81 75 751 3772; fax: +81 75 751 9416.

E-mail address: akio@kuhp.kyoto-u.ac.jp (A. Ikeda).

1388-2457/$30.00
doi:10.1016/j.clinph.2006.03.029

et al., 1990). As for the generator mechanism of giant SEPs, previous study by means of simultaneous recording of SEPs and somatosensory evoked magnetic fields (SEFs) showed that abnormal hyperexcitability involves both primary somatosensory and motor cortices (SI and MI, respectively) (Mima et al., 1998). However, the generator sources of giant SEPs have not been fully understood.

In the present study, we investigated the giant SEPs recorded from chronically implanted subdural electrodes in order to clarify the generator mechanism and the hyperexcitability of SI and MI in a patient with intractable focal epilepsy manifesting cortical reflex myoclonus. Only the abstract for this objective appeared elsewhere (Hitomi et al., 2004), and other electrophysiological and clinical features of the patient are described elsewhere for an entirely different purpose (Matsumoto et al., 2005; Mikuni et al., 2005; Nakagawa et al., in press).

2. Patient and methods

A 31-year-old man had intractable focal seizures and cortical reflex myoclonus involving the left foot due to focal cortical dysplasia in the right parasagittal central region. The patient was on many kinds of anticonvulsants, such as carbamazepine (800 mg/day), phenytoin (300 mg/day), phenobarbital (80 mg/day), zonisamide (700 mg/day) and clobazam (10 mg/day). By video-EEG monitoring, the epileptogenic zone was defined at and very close to the foot area of the right SI and MI. Clinically he had both positive and associated negative myoclonus and showed an enhanced long-loop transcortical reflex (C-reflex) to electrical stimulation of the left foot. Before implantation of the subdural electrodes, SEFs in response to stimulation of bilateral tibial nerves were recorded (passband: 0.07–200 Hz, sampling rate: 901 Hz) in the magnetically shielded room with the 122 first-order planar SQUID gradiometers (Neuromag122, Neuromag, Helsinki, Finland).

2.1. Scalp SEPs

Scalp SEPs in response to stimulation of bilateral tibial and sural nerves were recorded before implantation of the subdural electrodes and 20 days after the resective surgery. The electrical stimulus was presented as a constant voltage square-wave pulse of 0.2 ms duration, and interstimulus interval (ISI) was set to 2.9 s. It was delivered to the tibial nerve at the ankle and to the sural nerve below the lateral malleolus. Stimulus intensity was adjusted to 120% of motor threshold so as to produce a clear twitch of the hallux for the tibial nerve and to 300% of sensory threshold for the sural nerve. The scalp electrodes were placed at Fz, Cz and Pz based on the 10–20 International System, and were also placed at CPz, CP3 and CP4 defined as the midway between each corresponding pair of electrodes. All electrodes were referred to the linked earlobes (A1+A2). The bandpass filter of the amplifier was set to 1.6–3000 Hz, and sampling rate was set to 10,000 Hz. Three hundred responses for each session were averaged and at least two sets were recorded to confirm the reproducibility of the waveforms.

2.2. Epicortical SEPs

Single and paired pulse SEPs were recorded from subdural electrodes while the patient was undergoing invasive seizure monitoring and functional mapping. Informed consent was obtained based on the Clinical Research Protocol No. 79, approved by the Committee of Medical Ethics, Kyoto University Graduate School of Medicine. Single pulse SEPs were recorded by stimulation of the left tibial, peroneal and sural nerves. The condition of electrical stimulation for the left tibial and sural nerves were the same as those for the scalp SEP recording except for shorter ISI (1 s) in the epicortical recording. As for the left peroneal nerve, stimulus was delivered on the skin over the left fibular head and stimulus intensity was adjusted to 120% of motor threshold of the tibialis anterior muscle. All subdural electrodes were referred to the skin electrode on the left mastoid process. All other recording conditions were the same as those for scalp SEP recording.

Recovery functions of SEP response were studied by giving paired stimuli with various ISIs. Each pair of stimuli was delivered once every 3 s or longer. ISIs were set to 30, 40, 60, 80, 100, 120, 140, 160 and 200 ms. In order to maintain the same recording condition among different ISIs, stimuli with different ISIs were randomly delivered in the same recording session, and the single pulse stimuli were also intermixed among them. The SEP recovery function (SEP-R) of P1–N1 and N1–P2 components of the response to the second stimuli (SEP2) was calculated with respect to the response to the first stimuli (SEP1) for each ISI. Cortical excitability was judged to be non-suppressed when the ratio of SEP2/SEP1 was 100% or larger for both SI and MI. For statistical analysis, the Mann–Whitney U test was employed to compare the ratio of SEP2/SEP1 between non-suppressed ISIs data and suppressed one. The level of significance was set with P value of less than 5%.

3. Results

3.1. Scalp SEPs

Scalp SEPs following the left tibial nerve stimulation showed maximal cortical responses at CPz. As for the latencies, peaks of SEPs to the left foot stimulation were delayed (P1: 51.6 ms, N1: 63.8 ms and P2: 103.0 ms) as compared with the right foot stimulation (P1: 42.7 ms, N1: 55.8 ms and P2: 65.4 ms) (Table 1A, Fig. 1A and B). With regard to the amplitudes, P1–N1 and N1–P2 components for the left foot stimulation (P1–N1: 15.0 uV and N1–P2:

Table 1

Nerve	Electrode	Latency (ms)			Amplitude (μV)		
		P1	N1	P2	Baseline-P1	P1–N1	N1–P2
A scalp SEP							
Left tibial	CPz	51.6	63.8	103.0	6.0	15.0	17.1
Right tibial	CPz	42.7	55.8	65.4	0.1	3.6	2.7
Left sural	CPz	54.6	70.2	158.5	2.2	9.7	17.1
Right sural	CPz	50.1	61.4	135.0	0.1	3.0	8.6
B subdural SEP							
Left tibial	A19 (SI)	45.0	59.5	73.2	46.2	207.2	152.3
	B3 (MI)	49.6	64.8	82.4	2.4	86.5	86.6
Left peroneal	A19 (SI)	38.1	51.6	83.5	14.0	125.5	156.1
	B3 (MI)	43.8	59.9	88.2	47.3	258.8	276.8
Left sural	A19 (SI)	43.5	62.1	95.2	25.9	120.8	92.9
	B3 (MI)	49.1	68.7	97.2	32.0	104.5	102.1

17.1 μV) were about 4 times larger than those for the right foot stimulation (P1–N1: 3.6 μV and N1–P2: 2.7 μV) (Table 1A, Fig. 1A and B). P1–N1 for the left tibial nerve stimulation was compatible with 'giant' SEPs according to the previous study (P1–N1 amplitude being more than 11.4 μV (mean+3SD)) (Kakigi and Shibasaki, 1987b). As for the sural nerve stimulation, cortical components also showed delayed latencies and increased amplitudes to the left foot stimulation as compared with the right foot stimulation (Table 1A).

Twenty days after the resective surgery, scalp SEPs were recorded again. As for SEPs to the left tibial nerve stimulation, peak latencies (P1: 53.4 ms, N1: 70.2 ms and P2: 108.3 ms) were still delayed and amplitude of P1–N1 component (11.2 μV) was larger than that for the contralateral stimulation (2.4 μV). However, its amplitude

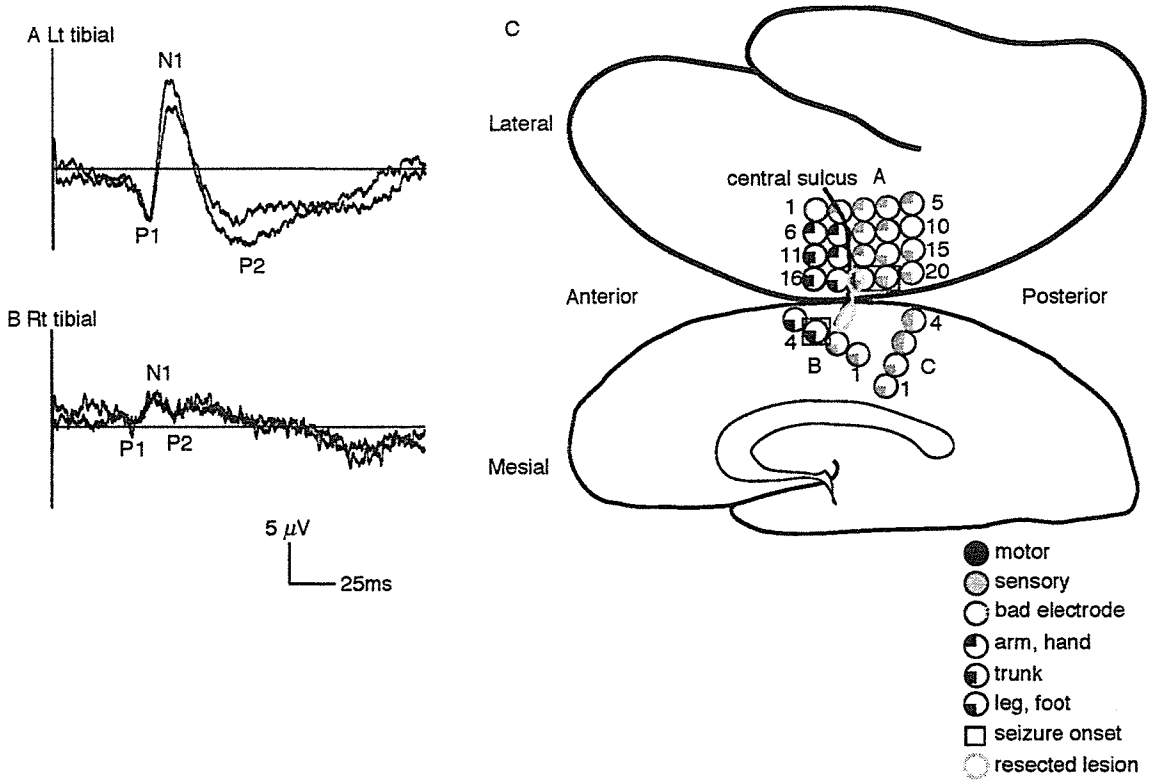

Fig. 1. Scalp recorded SEP waveforms at CPz to the left (A) and right (B) tibial nerve stimulation and the results of invasive functional mapping (C). In C, cortical functions beneath each subdural electrode are shown by symbols. B3, A18 and A19, as surrounded by bold squares, were defined as seizure onset area. Interictal spikes were frequently recorded at B2, B3, A18 and A19. A17, B3 and B4 corresponded to the foot or leg motor cortex, and A14, 15, 18-20, B1, 2 and C 1–4 corresponded to that of sensory cortex as determined by electrical stimulation. Gray bold circle and line indicated that the resected epileptogenic area of the cortical dysplasia was located in the posterior portion of the post-central gyrus reaching to the bottom of the right central sulcus.

became smaller in spite of the presence of craniotomy as compared with one before surgery.

As for the comparison between the scalp SEPs and SEFs to the left tibial nerve stimulation, peak latencies of P1 and N1 components at CPz were similar to those of SEFs (P1: 50.4 ms, N1: 62.4 ms).

3.2. Epicortical SEPs

Enhanced cortical components were recorded at A18 and A19 (SI) and at B3 (MI) (Fig. 1C). SEP waveforms among the 3 stimulated nerves (tibial, peroneal and sural) were similar in the latency of P1 and N1, and P1–N1 amplitude was equally enlarged (Table 1B). The peak latencies of the left peroneal nerve SEPs were shorter by 5–7 ms than those of tibial and sural nerve SEPs, since the former was stimulated at the fibular head whereas the latter two were stimulated at the ankle.

There was a consistent latency difference of each peak between SI and MI, although the waveforms of cortical components at SI (A19) and MI (B3) were similar (Fig. 2). Peak latencies of each component (P1, N1, P2) at SI (A19) were shorter than those at MI (B3) by about 6 ms on average (mean $\pm$ SD: 5.8 $\pm$ 2.1; ranging from 2.0 to 9.2); left tibial (6.4 $\pm$ 2.8; 4.6–9.2), peroneal (4.7 $\pm$ 2.4; 2.0–5.6) and sural (6.2 $\pm$ 1.9; 4.7–8.3). Peak latencies at SI (B2) were also shorter than those at MI (B3) by about 6 ms (6.0 $\pm$ 2.3; 2.0–9.9) despite the proximity of the recording site (Fig. 2). The P1–N1 amplitudes at both SI (A19) and MI (B3) were equally enhanced for the left tibial, peroneal and sural nerve stimulation (Table 1B).

The comparison between scalp and epicortical SEPs to the left tibial nerve stimulation showed similar morphology of P1 and N1 components, but the late components including P2 were different (Fig. 2A). A similar tendency was observed for the left sural nerve stimulation (Fig. 2B). Peak latencies of P1 and N1 components at CPz were longer than those at SI (A19) by about 4–11 ms to the left tibial (P1: 6.6 ms, N1: 4.3 ms) and sural (P1: 8.1 ms, N1: 11.1 ms) nerve stimulation. By contrast, the time difference between MI (B3) and CPz was much less than that between SI and CPz; left tibial (P1: 2.0 ms, N1: 1.0 ms) and sural (P1: 5.5 ms, N1: 1.5 ms) nerve stimulation (Table 1, Fig. 2).

As for the SEP-R of P1–N1 and N1–P2 components, the SEP2 was less than 100% of the SEP1 at SI (A19) and MI (B3) with all the ISIs examined in the present study (Fig. 3), as judged by normal range (within mean $\pm$ 3SD of those obtained from normal subjects) in previous scalp-recorded, paired SEP study (Ugawa et al., 1991). In detail, the SEP2 was less than 60% of the SEP1 at SI (A19) and MI (B3) at ISI of 30–200 ms except for the ISIs of 40 ms (80.7% at SI and 92.0% at MI for P1–N1 component, 94.5% at SI and 82.4% at MI for N1–P2 component) and of 200 ms (77.2% at SI and 63.0% at MI, 94.5% at SI and 91.3% at MI) (Fig. 3). The degree of

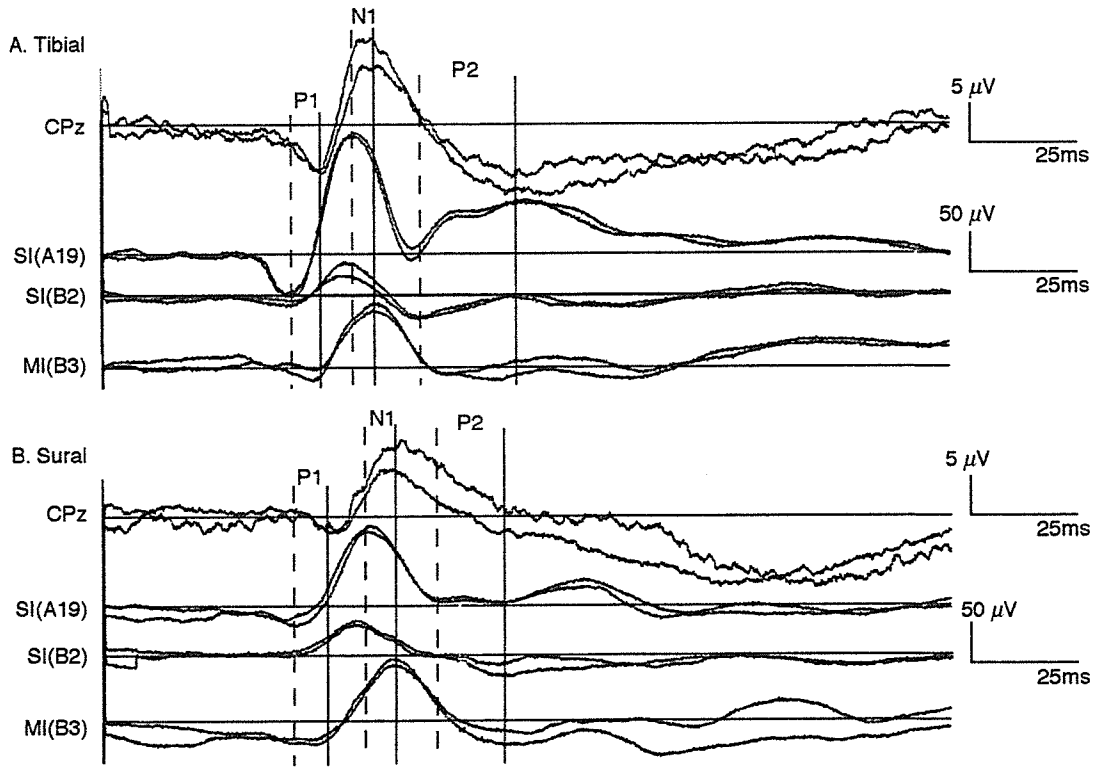

Fig. 2. Scalp (CPz) and subdurally (SI and MI) recorded SEPs to the left tibial (A) and sural (B) nerve stimulation. Vertical solid lines show peaks of each component (P1, N1, P2) at CPz and vertical dotted lines show those at SI (A19 and B2) to the left tibial and sural nerve stimulation. The peak latencies were consistently longer at MI as compared with SI, and the latencies at MI were similar to those at CPz.